Imprint of Alpha Clustering

in Relativistic Light Ion collisions

Hadi Mehrabpour

Intersection of nuclear structure and high-energy nuclear collisions
YITP, April 13-24, 2026

Fundamental structure of atomic nuclei

Chun Shen, Quark Matter 2025

- Multipole deformations
- Clustering
- Neutron skin/halo
- …

$$\rho(r,\phi,\theta) \propto \frac{1}{1+\exp[(r-R(\phi,\theta)/a]}$$

$$R(\phi,\theta) = R_0[1+\beta_2^{WS}(\cos(\gamma)Y_{20}(\theta)+\sin(\gamma)Y_{22}(\theta,\phi))+\beta_3^{WS}Y_{30}(\theta)+\beta_4^{WS}Y_{40}(\theta)]$$

STAR Collaboration, Nature 635, 67-72 (2024)

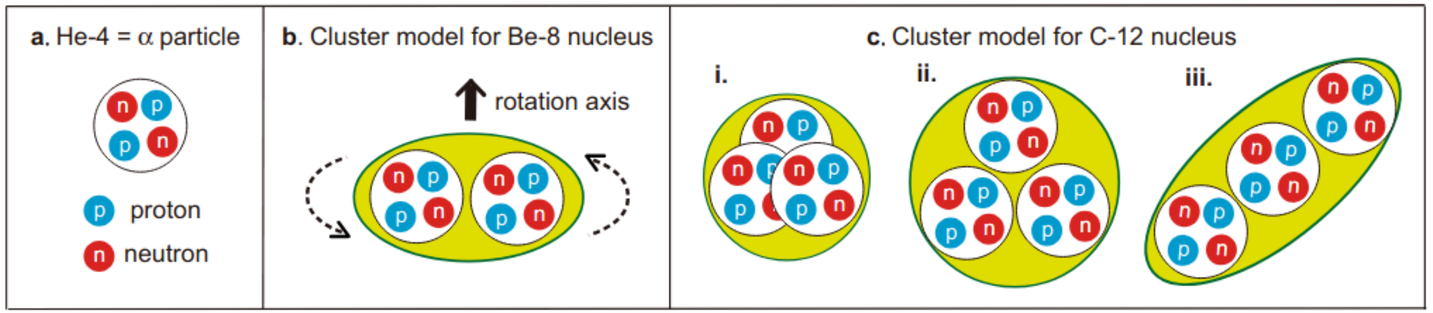

T.Otsuka et al., Nature Commun 13, 2234 (2022)

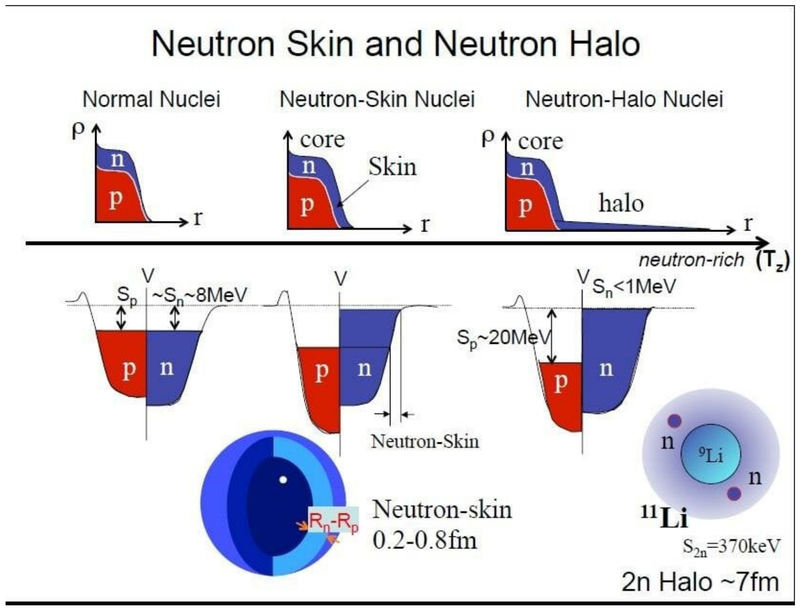

PREX Collaboration, PRL 126, 172502 (2021)

It is the required bridge between:

- how the universe makes elements,
- how we harness nuclear energy,
- and neutrinoless double beta decay.

Talk by Jiangming Yao, April 13, 10:00 PM
Talk by Kenta Hagihara, April 13, 11:00 PM
Talk by Xin Zhang, April 13, 14:30 PM

Not all Forests are beautiful!

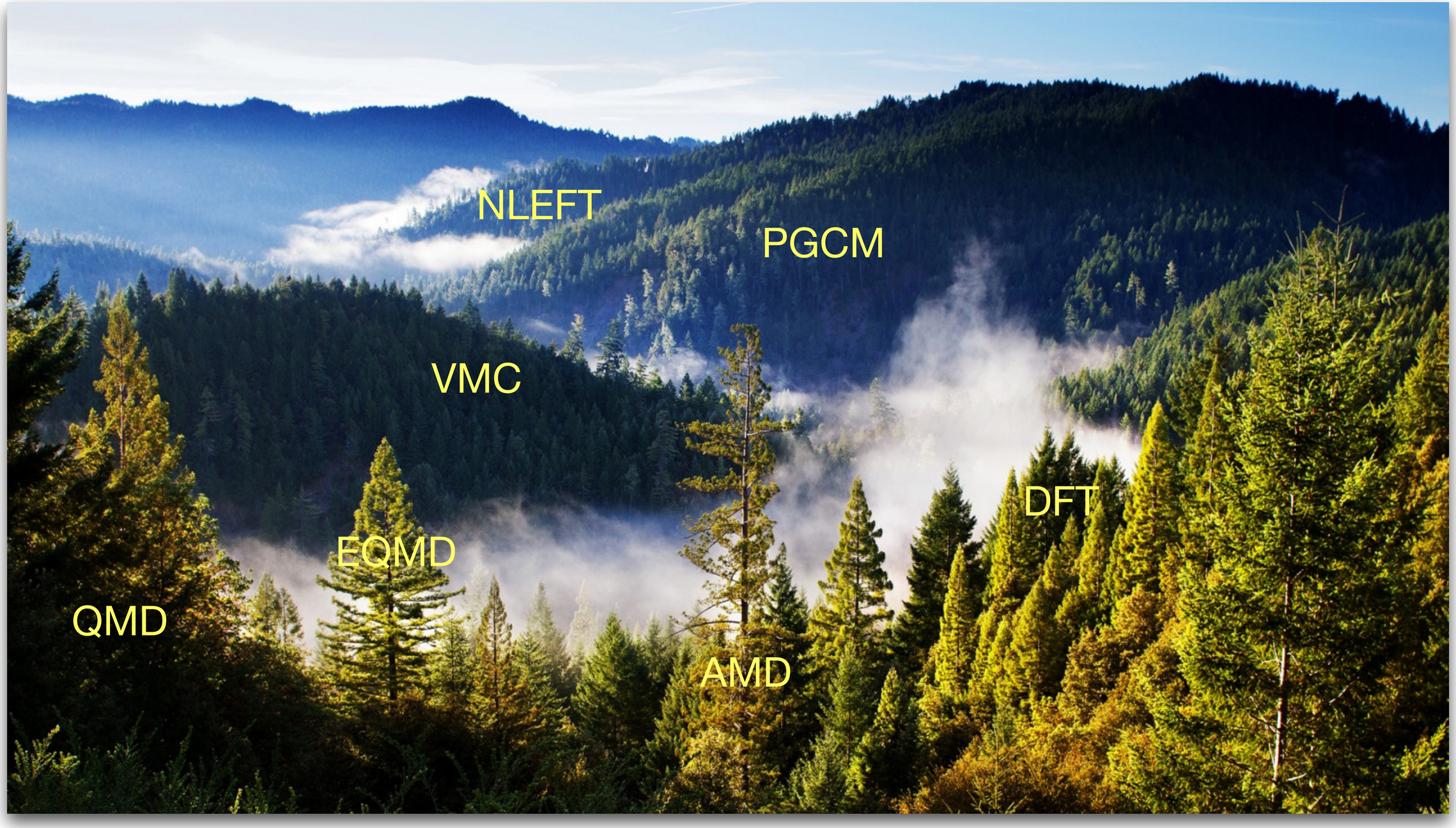

High Energy Experiments

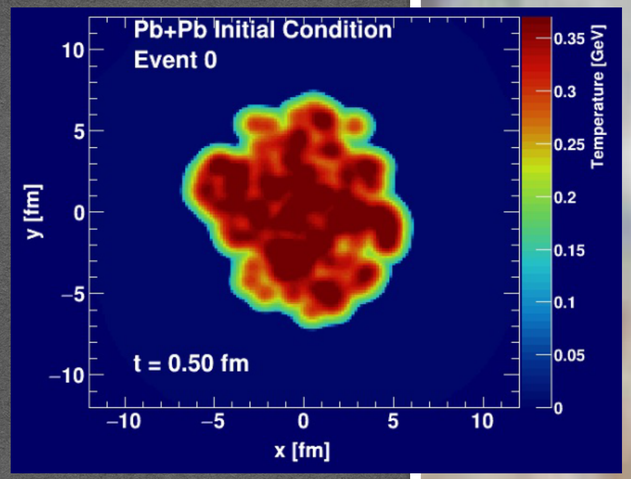

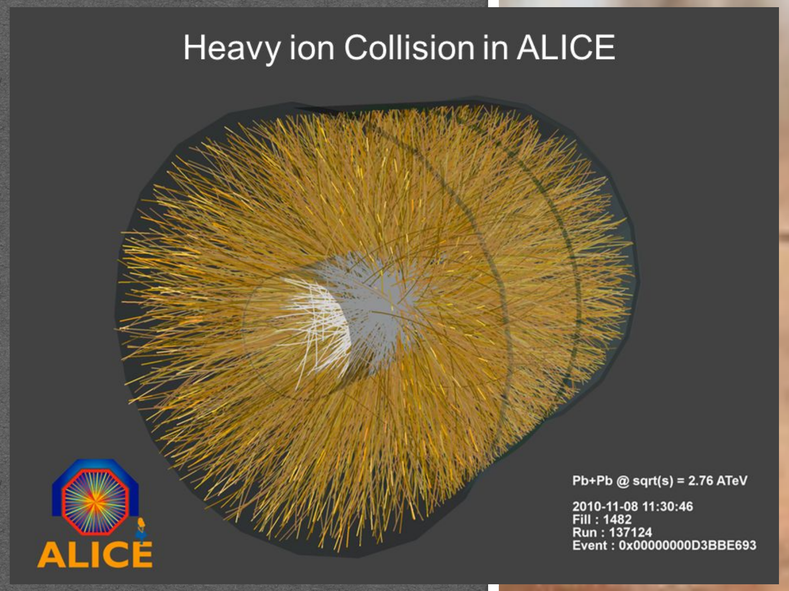

Standard Model of HIC

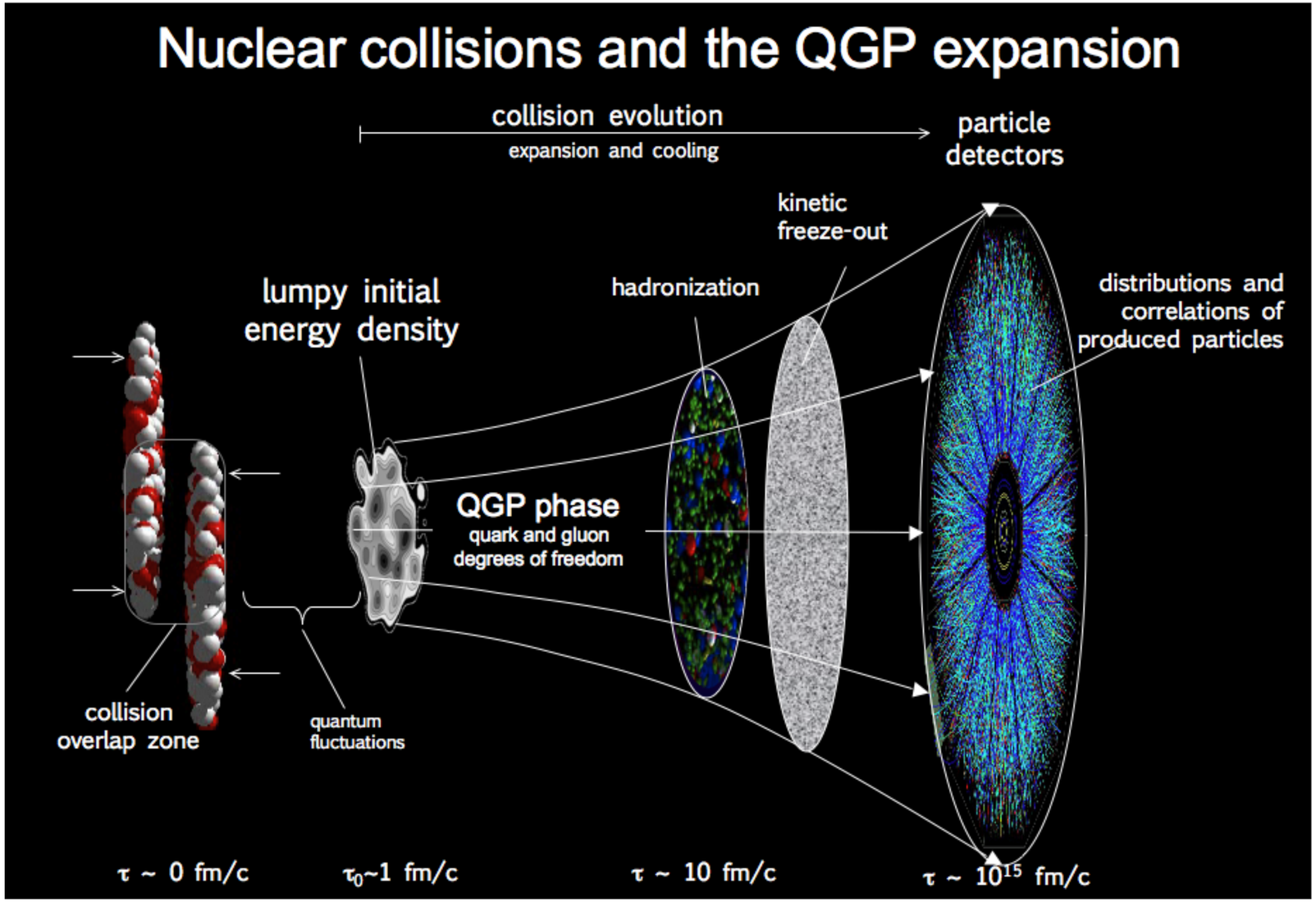

P.Sorensen, arXiv: 0905.0174

Can we reconstruct information about nuclear structures from HIC measurements?

❃ Shape of the fireball: Anisotropic flow

$$V_n \propto \mathscr{E}_n$$

H.Niemi et al., PRC 87 (2013) 5, 054901

❃ Size of the fireball: Radial flow

$$\langle p_T \rangle \propto \frac{1}{R} \quad \text{and} \quad \langle p_T \rangle \propto E$$

G.Giacalone et al., PRC 103 (2021) 2, 024909

Strong Collective Correlation of Nucleons

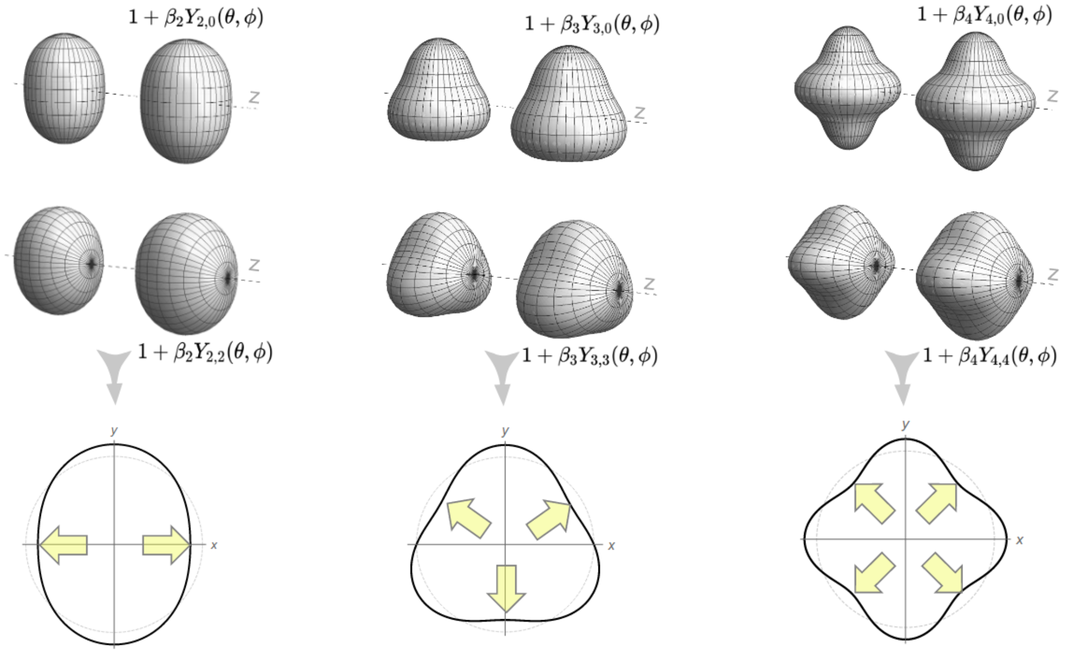

J.Jia, PRC 105 (2021) 014905

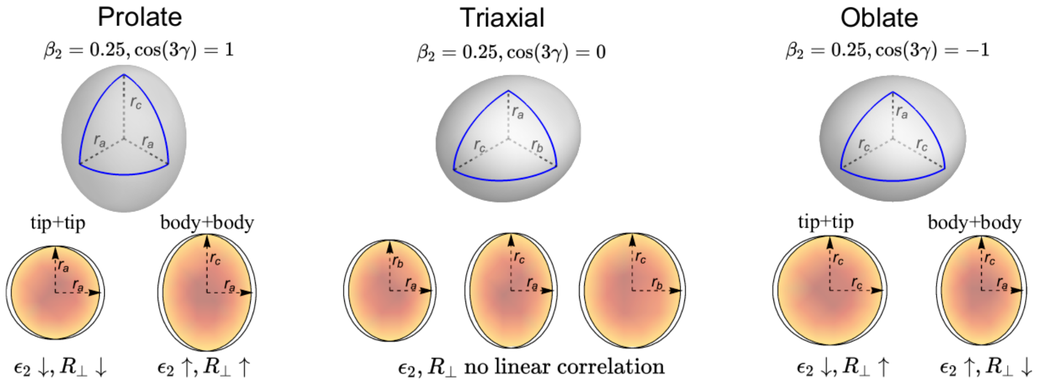

J.Jia, PRC 105 (2022) 4, 044905

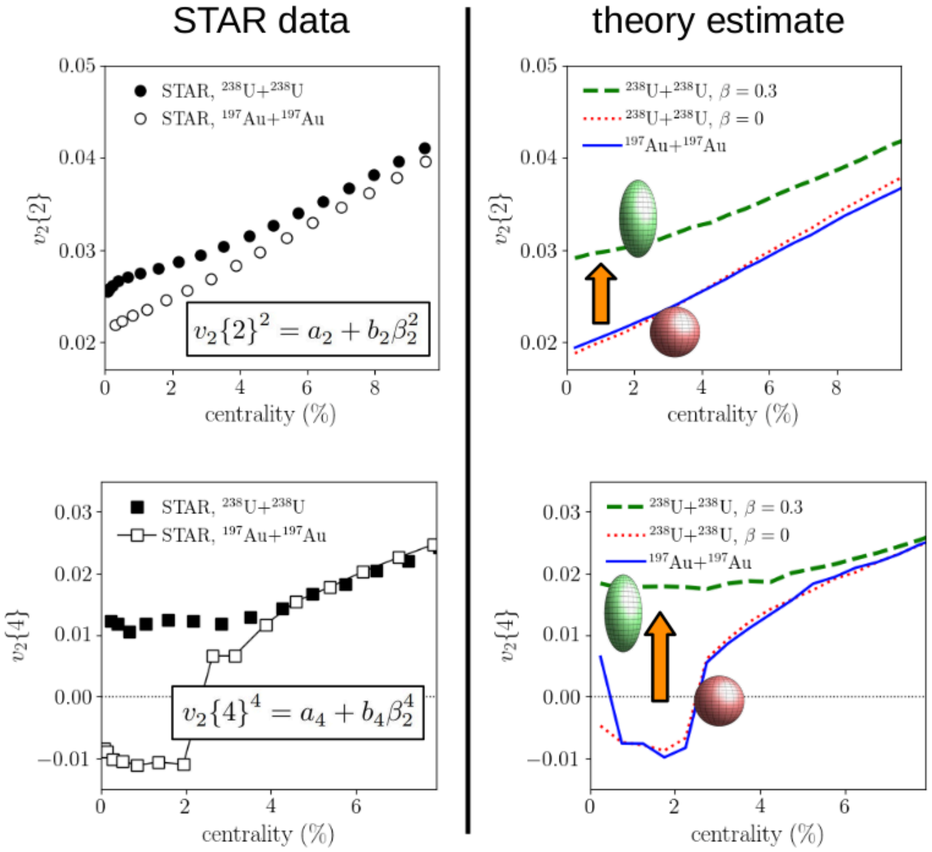

STAR Collaboration, PRL 115 (2015) 222301

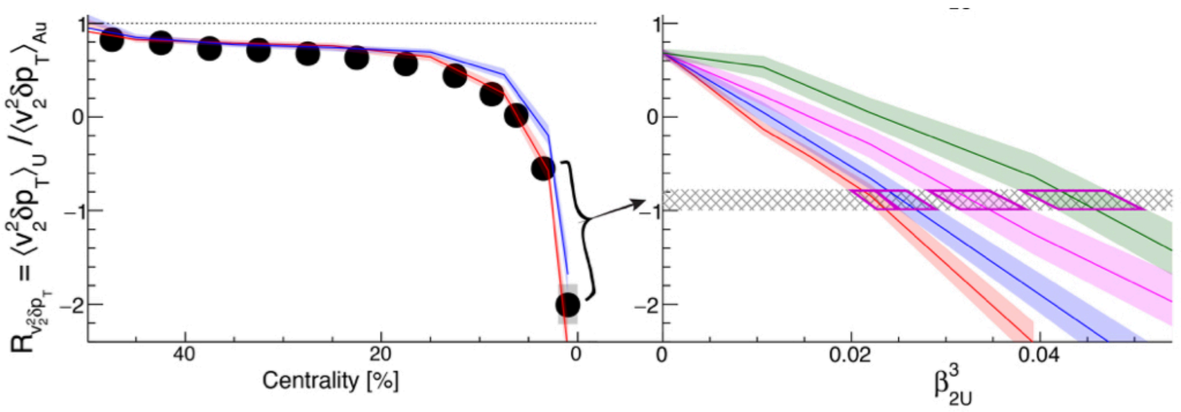

STAR Collaboration, Nature 635 (2024) 8037

Opportunity of Light Ion Collisions

- Connecting ***ab initio*** model with relativistic nuclear collisions

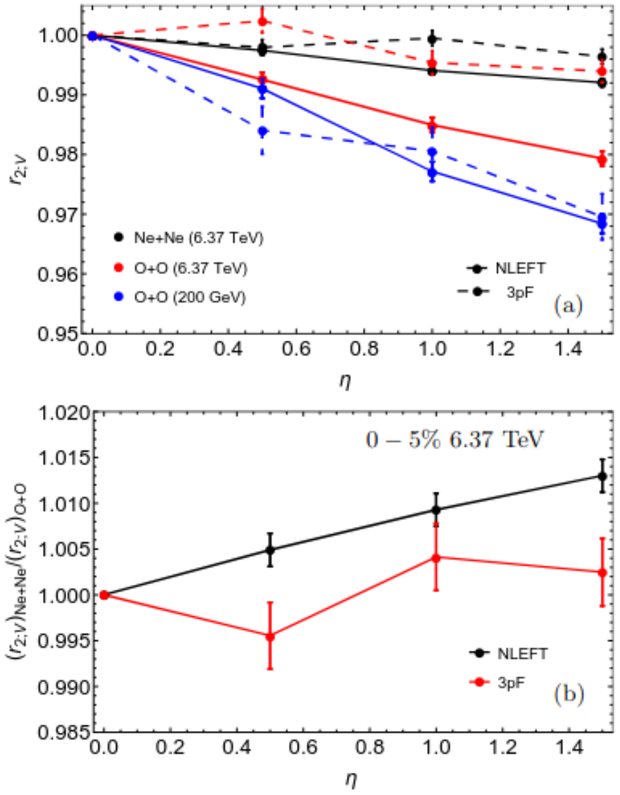

HM, A.Saha, EPJC 85 (2025) 1284

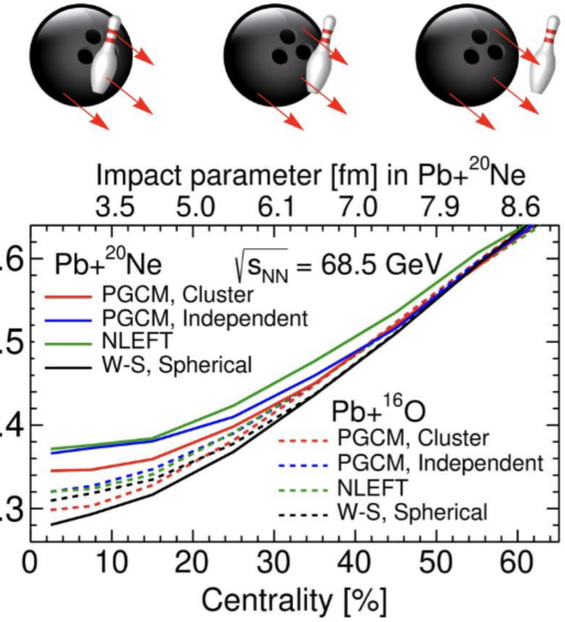

G.Giacalone et al., PRL 134 (2025) 082301

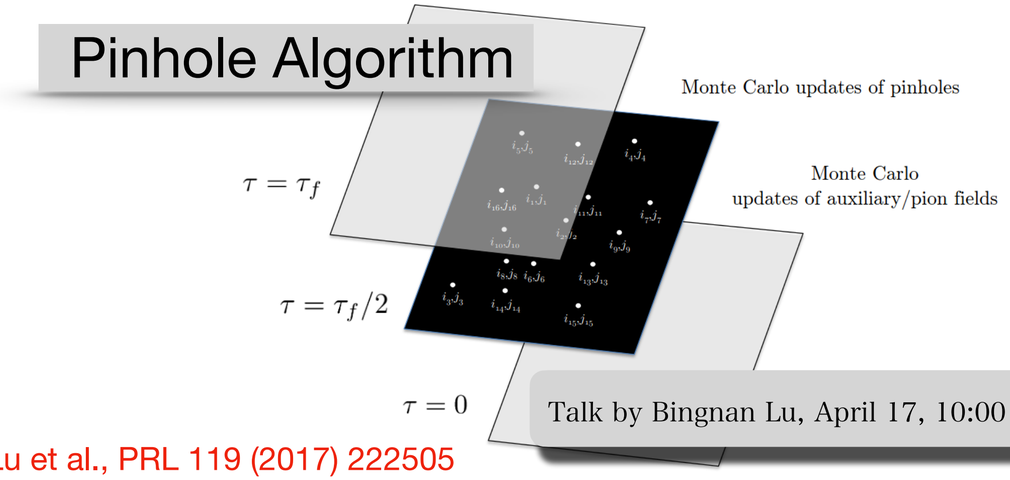

B.N.Lu et al., PRL 119 (2017) 222505

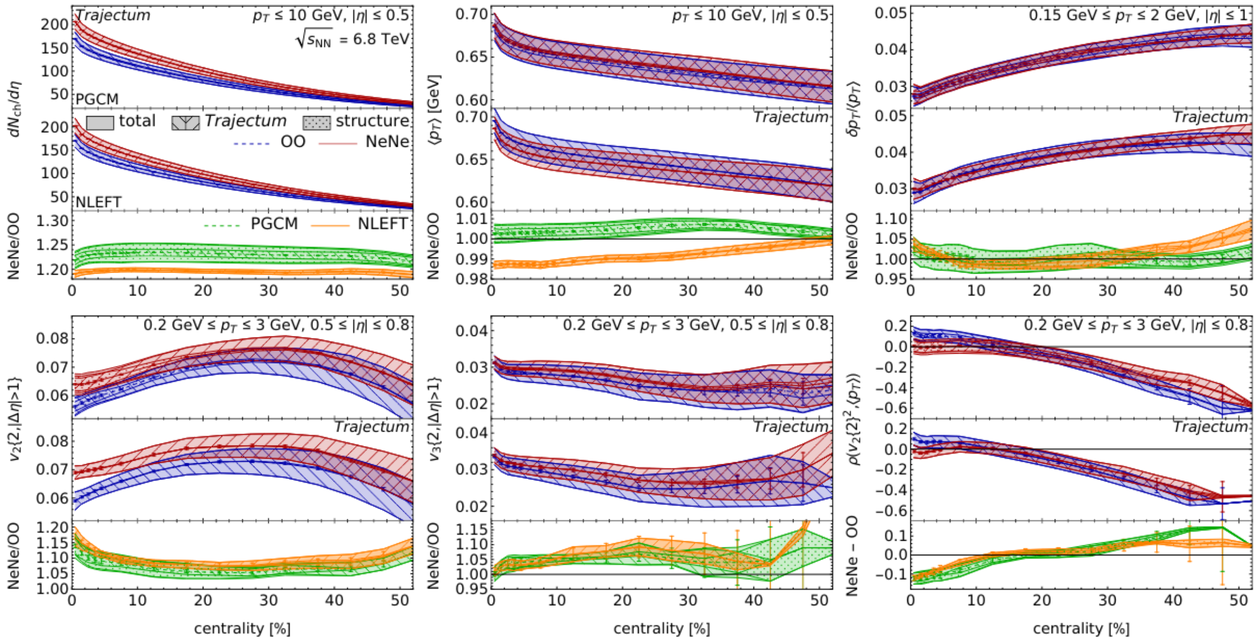

G.Giacalone et al., PRL 135 (2025) 012302

Opportunity of Light Ion Collisions

Evidence of nuclear geometry-driven anisotropic flow in OO and Ne–Ne collisions at $\sqrt{s_{\mathrm{NN}}}$ = 5.36 TeV

ALICE Collaboration*

Abstract

tion physics, governed by quantum chromodynamics (QCD), is ark–gluon plasma (QGP) form in small collision systems involv- than heavy ions. Collisions of light ions such as ^{16}O and ^{20}Ne the emergence of collective behavior in QCD matter. This Let- of elliptic (v_2) and triangular (v_3) flow of charged particles in at a center-of-mass energy per nucleon pair of $\sqrt{s_{\mathrm{NN}}} = 5.36$ TeV odynamic model predictions, explicitly incorporating the nuclear a good agreement with the flow measurements presented. The Ne–Ne collisions relative to OO collisions, driven by the nuclear nce of utilizing light nuclei with well-defined geometric shapes These findings support the presence of nuclear geometry-driven isions at the LHC.

First measurement of pseudorapidity distributions of charged hadrons in oxygen-oxygen collisions at $\sqrt{s_{\mathrm{NN}}} = 5.36$ TeV with CMS

The CMS Collaboration

Abstract

t of the charged hadron pseudorapidity (η) distri- ions at a nucleon-nucleon center-of-mass energy of re recorded by the CMS experiment at the LHC in rged hadrons produced in the range $|\eta| < 2.4$ are pixel detector. The midrapidity particle density as is also reported. In the 5% most central collisions, the range $|\eta| < 0.5$ is found to be 135 ± 3 (syst), with The data are compared to previous measurements of sions at similar collision energies and several Monte studies of the dependence of particle production on ion geometry, and the size of the colliding nuclei are

Measurement of the azimuthal anisotropy of charged particles in $\sqrt{s_{\mathrm{NN}}}$ = 5.36 TeV ^{16}O+^{16}O and ^{20}Ne+^{20}Ne collisions with the ATLAS detector

The ATLAS Collaboration

s the first measurements of the azimuthal anisotropy coefficients v_n, which rder Fourier modulation of charged-particle azimuthal distributions, for 5.36 TeV ^{16}O + ^{16}O and ^{20}Ne + ^{20}Ne collisions recorded with the ATLAS ge Hadron Collider in 2025. The v_n coefficients are measured as a function entum (p_{T}), collision centrality, and event multiplicity. They are extracted entary methods: two-particle correlations with a template-fit subtraction of ow contributions, and four-particle subevent cumulants, which intrinsically effects and provide sensitivity to flow fluctuations. The results show a clear $> v_4$ and a non-monotonic dependence on p_{T}, reaching a maximum around with trends observed in heavy-ion collisions. Detailed comparisons between ystems reveal an enhanced v_2 in central ^{20}Ne + ^{20}Ne collisions, consistent ations based on the predicted prolate deformation of neon nuclei, in contrast hedral structure predicted for oxygen. The four-particle cumulant results vent-by-event fluctuations and provide the greatest sensitivity to nuclear se measurements can place new constraints on the initial geometry and the ponse in light-ion collisions, offering valuable input for models of nuclear

Unveiling the shape of the ^{20}Ne nucleus by measuring the flow coefficients with cumulants in PbNe and PbAr collisions at $\sqrt{s_{\mathrm{NN}}} = 70.9$ GeV

LHCb collaboration†

Abstract

The anisotropic flow coefficients v_n quantify the collective medium response to the initial spatial anisotropy of the overlapping region in ion collisions and serve as sensitive probes of both the medium properties and shape of nuclear initial states. In this analysis, the v_2 and v_3 parameters of prompt charged particles are measured using the multiparticle cumulant method in fixed-target PbNe and PbAr collisions at $\sqrt{s_{\mathrm{NN}}} = 70.9$ GeV, collected by LHCb using the SMOG2 gas-target system during the 2024 LHC lead-beam run. The cumulant method is first validated using 2018 PbPb collision data, successfully reproducing previous measurements obtained via the two-particle correlation method. Results for the fixed-target collisions are then presented, showing a significantly larger value of the elliptic flow coefficient v_2 in central PbNe with respect to PbAr collisions. This is qualitatively consistent with 3+1D hydrodynamic predictions including *ab-initio* descriptions of the nuclear structure. The results provide the first experimental confirmation of the distinctive bowling-pin shape of the ground-state ^{20}Ne nucleus, validating at the same time the hydrodynamic description of the hot medium formed in high-energy collisions involving light ions.

LHC ⟷ RHIC

Talk by Chunjian Zhang, April 15, 11:00 AM

Light ion collisions at the LHC-2025

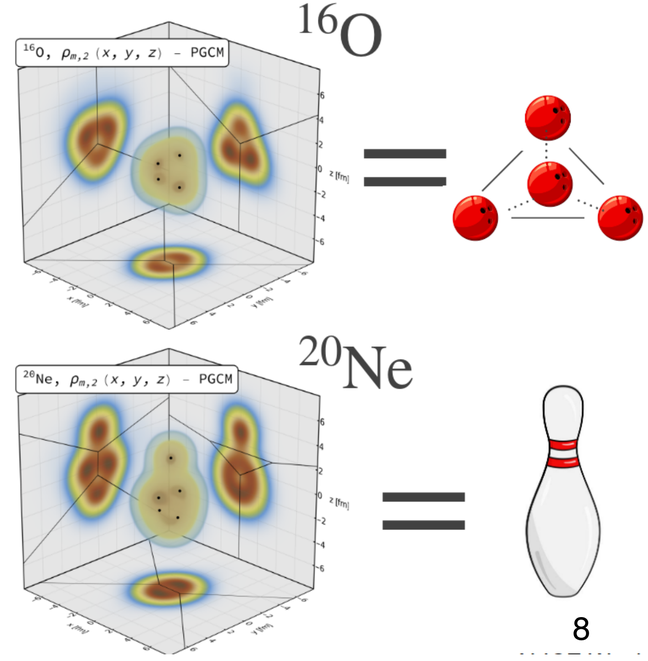

Clustering Model

George Gamow, Nature 130, 648 (1932)

M.Rybczynski et al., PRC 97 (2018) 034912
Y.Wang et al., PRC 109, L051904 (2024)
D.Behera et al., PRC 109, 014902 (2024)
Z.Lu et al., PLB 868, 139698 (2025)
C.Zhang et al., PLB 862, 139322 (2025)
L-M.Liu et al., PRC 111, L021901 (2025)
J.P.Blaizot & G.Giacalone, EPJA 61 (2025) 9, 220
J-Y.Hu et al., 2507.01493
P.Li et al., 2511.23293
X.Fan et al., 2511.23293
J.P.Blaizot et al., 2512.18926
…

Talk by Oscar Garcia-Montero, April 15, 10:00 AM
Talk by Chunjian Zhang, April 15, 11:00 AM
Talk by Giuliano Giacalone, April 20, 10:00 AM
Talk by Weiyao Ke, April 20, 11:00 AM

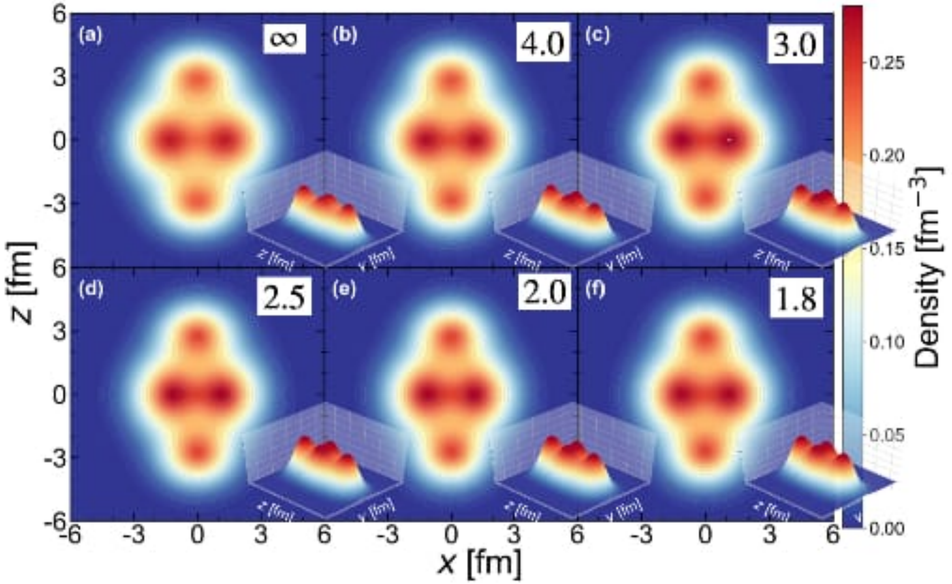

Talk by Jiangming Yao, April 13, 10:00 AM

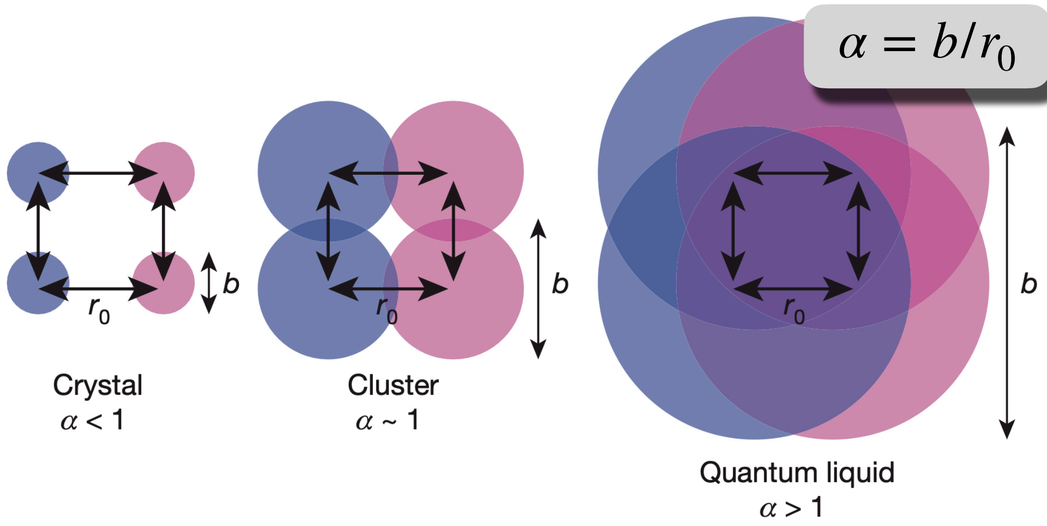

JP. Ebran et al., Nature 487, 341–344 (2012)

General Picture: A Rigid-Rotor Model

❃ Can we find an approximate yet realistic analytical model of the collision process?

- The leading dependency of final-state observables on nuclear structure of two colliding nuclei
- Symmetric and asymmetric collisions
- Light and heavy nuclei collisions

Talk by Giuliano Giacalone, April 20, 10:00 AM

❃ Approach G.Giacalone, EPJA 59 (2023) 297

n-body particle densities:

A-nucleon ground-state wave function

$$\rho^{(n)}(\mathbf{r}_1, \mathbf{r}_2, \cdots, \mathbf{r}_n) = \int_{\mathbf{r}_{n+1},\cdots,\mathbf{r}_A} |\Psi(\mathbf{r}_1, \mathbf{r}_2, \cdots, \mathbf{r}_A)|^2$$

Transverse n-body density of nucleons: M.Alvioli et al., PLB 680, 22 (2009)

$$\rho_{\perp}^{(n)}(\mathbf{r}_{1\perp}\ldots, \mathbf{r}_{n\perp}) = \int_{z_1,\ldots,z_n} \rho^{(n)}(\mathbf{r}_1, \mathbf{r}_2, \cdots, \mathbf{r}_n)$$

n-body Operators:

T.Duguet et al., PRL 135 (2025) 182301

$$\langle \hat{R}_2 \rangle = \langle r_\perp^2 \rangle = 2R_0^2 + \mathcal{O}(\beta_2^2)$$

$$\langle \hat{\mathscr{E}}_2 \rangle = \left\langle r_{1\perp}^n r_{2\perp}^n e^{in(\phi_1-\phi_2)} \right\rangle = \frac{6}{\pi} R_0^4 \beta_2^2 + \mathcal{O}(\beta_2^3)$$

HM, G.Giacalone, M.Luzum, 2604.00619

$$\langle \hat{T} \rangle = \left\langle r_{1\perp}^2 r_{2\perp}^2 r_{3\perp}^2 e^{i2(\phi_2-\phi_3)} \right\rangle - \left\langle r_\perp^2 \right\rangle \left\langle r_{1\perp}^2 r_{2\perp}^2 e^{i2(\phi_1-\phi_2)} \right\rangle$$

$$= \frac{12\sqrt{5}R_0^6}{7\pi^{3/2}} \beta_2^3 \cos(3\gamma) + \mathcal{O}(\beta_2^4)$$

General Picture: A Rigid-Rotor Model

❃ Can we find an approximate yet realistic analytical model of the collision process?

- The leading dependency of final-state observables on nuclear structure of two colliding nuclei
- Different symmetric and asymmetric collisions
- Small and large systems

Talk by Giuliano Giacalone, April 20, 10:00 AM

❃ Approach G.Giacalone, EPJA 59 (2023) 297

The density of overlapping area: J.S.Moreland et al., PRC 92, 011901 (2015)

$$\epsilon(\mathbf{r}_\perp) = \left(T(\mathbf{r}_\perp)T'(\mathbf{r}_\perp)\right)^p = \left(\sum_{i=1}^{A} g(\mathbf{r}_\perp - \xi_i) \sum_{j=1}^{B} g'(\mathbf{r}_\perp - \xi_j)\right)^p$$

Profile of a nucleon located at position ξ_i in the transverse plane

A point in the transverse plane after the collision takes place

Impact parameter is zero

$p = 1$

k-body correlations: J.P.Blaizot et al., PLB 738, 166 (2014)

$$\langle \epsilon(\mathbf{r}) \rangle = \left[A \int_\xi \rho_\perp^{(1)}(\xi) g(\mathbf{r} - \xi) \right]^2$$

$$\langle \epsilon(\mathbf{r}_1)\epsilon(\mathbf{r}_2) \rangle = \left[A \int_\xi \rho_\perp^{(1)}(\xi) g(\mathbf{r}_1 - \xi) g(\mathbf{r}_2 - \xi) + A(A-1) \int_{\xi_1,\xi_2} \rho_\perp^{(2)}(\xi_1, \xi_2) g(\mathbf{r}_1 - \xi_1) g(\mathbf{r}_2 - \xi_2) \right]^2$$

$\vdots$

Light Nuclei: Alpha Clustering

HM, PRC 113 (2026) 3, 034909

❃ Distribution of nucleons in each cluster

M.Rybczynski et al., PRC 97 (2018) 034912

$$\rho_\alpha(\vec{r}) = \left(\frac{3}{2\pi r_L^2}\right)^{3/2} \exp\left[-\frac{3(\vec{r}-\vec{L}_i)}{2r_L^2}\right]$$

$\vec{L}_i$: Position of the center of the cluster i

r_L: Root-mean-square radius of the clusters

❃ Transverse densities:

- One-body density:

$$\rho_\perp^{(1)}(\mathbf{r}) = \sum_{i=1}^{N_\alpha} \langle \rho_{\alpha_i}(\mathbf{r},\Omega)\rangle_\Omega = \frac{3}{2\pi r_L^2} e^{-\frac{3|\mathbf{r}|^2}{2r_L^2}} \sum_{i=1}^{N_\alpha} \left\langle \exp\left[-\frac{f_i - 2(x\,h_{x,i} + y\,h_{y,i})}{2r_L^2/3}\right]\right\rangle_\Omega$$

- Two-body density:

$$\rho_\perp^{(2)}(\mathbf{r},\mathbf{r}') = \frac{9}{4\pi^2 r_L^4} e^{-\frac{3(|\mathbf{r}|^2+|\mathbf{r}'|^2)}{2r_L^2}} \sum_{i,j}^{N_\alpha} \left\langle \exp\left[-\frac{f_i - 2(x\,h_{x,i} + y\,h_{y,i}) + f_j - 2(x'\,h_{x',j} + y'\,h_{y',j})}{2r_L^2/3}\right]\right\rangle_\Omega$$

$\Omega = (a_1, a_2, a_3)$

$c_i = \cos a_i$ *and* $s_i = \sin a_i$

$$f_i = |\vec{L}_i|^2 - (L_{z,i}\,c_2 + (-L_{y,i}\,c_1 + L_{x,i}\,s_1)\,s_2)^2$$

$$h_{x,i} = (L_{y,i}\,c_1\,c_2 - L_{x,i}\,c_2\,s_1 + L_{z,i}\,s_2)\,s_3 + (L_{y,i}\,s_1 + L_{x,i}\,c_1)\,c_3$$

$$h_{y,i} = (L_{y,i}\,c_1\,c_2 - L_{x,i}\,c_2\,s_1 + L_{z,i}\,s_2)\,c_3 - (L_{y,i}\,s_1 + L_{x,i}\,c_1)\,s_3$$

Light Nuclei: Alpha Clustering

HM, PRC 113 (2026) 3, 034909

❃ Distribution of nucleons in each cluster

M.Rybczynski et al., PRC 97 (2018) 034912

$$\rho_\alpha(\vec{r}) = \left(\frac{3}{2\pi r_L^2}\right)^{3/2} \exp\left[-\frac{3(\vec{r}-\vec{L}_i)}{2r_L^2}\right]$$

$\vec{L}_i$: Position of the center of the cluster i

r_L: Root-mean-square radius of the clusters

❃ Transverse densities:

- One-body density:

$$\rho_\perp^{(1)}(\mathbf{r}) = \sum_{i=1}^{N_\alpha} \langle \rho_{\alpha_i}(\mathbf{r},\Omega)\rangle_\Omega = \frac{3}{2\pi r_L^2} e^{-\frac{3|\mathbf{r}|^2}{2r_L^2}} \sum_{i=1}^{N_\alpha} \left\langle \exp\left[-\frac{f_i - 2(x\,h_{x,i} + y\,h_{y,i})}{2r_L^2/3}\right]\right\rangle_\Omega$$

- Two-body density:

Intra-Cluster: $\rho_{\perp,1}^{(2)}(\mathbf{r},\mathbf{r}') = \sum_{i=1}^{N_\alpha} \left\langle \rho_\perp^{(\alpha_i)}(\mathbf{r},\Omega)\rho_\perp^{(\alpha_i)}(\mathbf{r}',\Omega)\right\rangle_\Omega$

Inter-Cluster: $\rho_{\perp,2}^{(2)}(\mathbf{r},\mathbf{r}') = \sum_{i\neq j}^{N_\alpha} \left\langle \rho_\perp^{(\alpha_i)}(\mathbf{r},\Omega)\rho_\perp^{(\alpha_j)}(\mathbf{r}',\Omega)\right\rangle_\Omega$

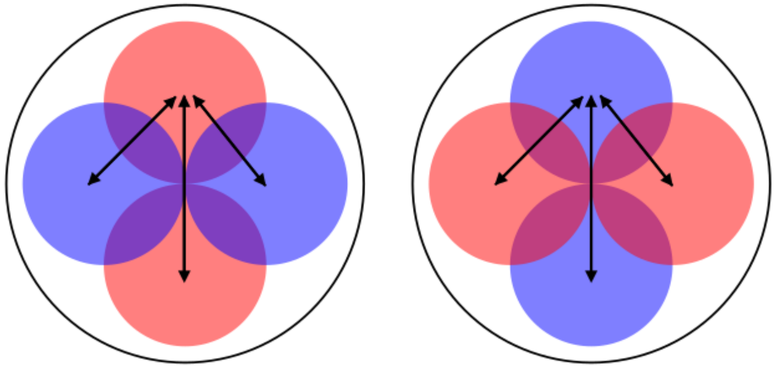

Intra-Cluster

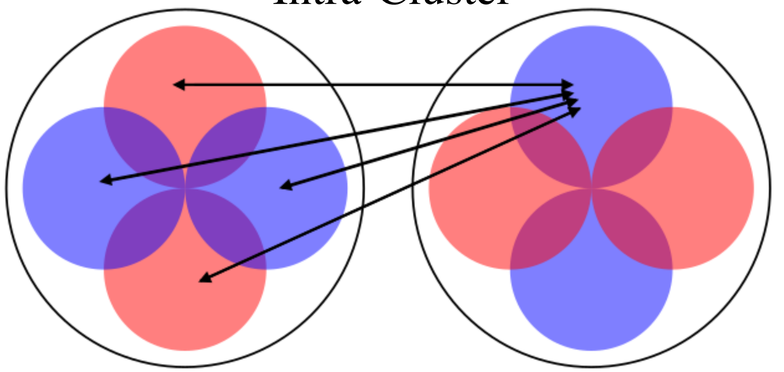

Inter-Cluster

Light Nuclei: Alpha Clustering

HM, PRC 113 (2026) 3, 034909

❃ Two-point function:

$$\langle \epsilon(\mathbf{r},\Omega,\Omega')\epsilon(\mathbf{r}',\Omega,\Omega')\rangle = \langle \sum_{s,t=1}^{A,B} \mathcal{G}(\mathbf{r}-\xi_s)\mathcal{G}(\mathbf{r}-\xi_t) \sum_{n,m=1}^{A,B} \mathcal{G}(\mathbf{r}'-\xi_n)\mathcal{G}(\mathbf{r}'-\xi_m)\rangle$$

$$= \langle \sum_{s,n=1}^{A} \mathcal{G}(\mathbf{r}-\xi_s)\mathcal{G}(\mathbf{r}'-\xi_n) \sum_{t,m=1}^{B} \mathcal{G}(\mathbf{r}-\xi_t)\mathcal{G}(\mathbf{r}'-\xi_m)\rangle$$

$$= \Big[A \int_\xi \rho_\perp^{(1)}(\xi) g(\mathbf{r}-\xi) g(\mathbf{r}'-\xi) + (A^2-A) \int_\xi \int_{\xi'} \rho_\perp^{(2)}(\xi,\xi') g(\mathbf{r}-\xi) g(\mathbf{r}'-\xi') \Big]^2$$

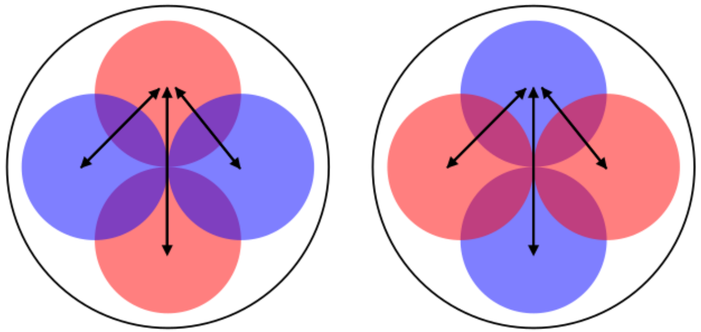

Intra-Cluster

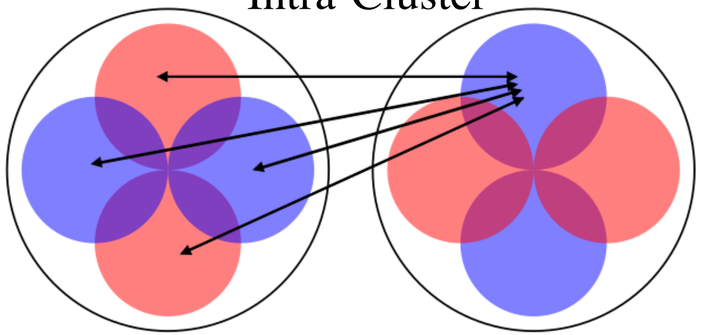

Inter-Cluster

$$= \Big[A' N_\alpha \mathcal{I}^{(1)}(\mathbf{r},\mathbf{r}',\Omega) + N_\alpha (A'^2 - A') \mathcal{I}_1^{(2)}(\mathbf{r},\mathbf{r}',\Omega) + A'^2 N_\alpha (N_\alpha - 1) \mathcal{I}_2^{(2)}(\mathbf{r},\mathbf{r}',\Omega) \Big]^2$$

$A' = 4$

One-body density | Intra-Cluster | Inter-Cluster

Light Nuclei: Nucleon Configurations

❇ Projected Generator Coordinate Method (PGCM)

M.Frosini et al., EPJA 58, 64 (2022)

- ❖ Ab initio formalism
- ❖ N^3LO EFT Hamiltonian
- ❖ Particle-number projected one-body density from intrinsic Hartree-Fock-Bogoliubov state

Talk by Thomas Duguet, April 16, 10:00 AM

❇ Nuclear Lattice Effective Field Theory (NLEFT)

U.-G.Meißner et al., PRL 119, 222505 (2017)

- ❖ Effective field theory + lattice Monte Carlo
- ❖ Well-suited to probe clustering effects
- ❖ Nuclear many-body correlations to all orders preserved

Talk by Bingnan Lu, April 17, 10:00 AM

❇ Variational Mone Carlo (VMC)

D.Lonardoni et al., PRC 97, 044318 (2018)

- ❖ N^2LO chiral EFT Hamiltonian
- ❖ Including shorts-range repulsive effects

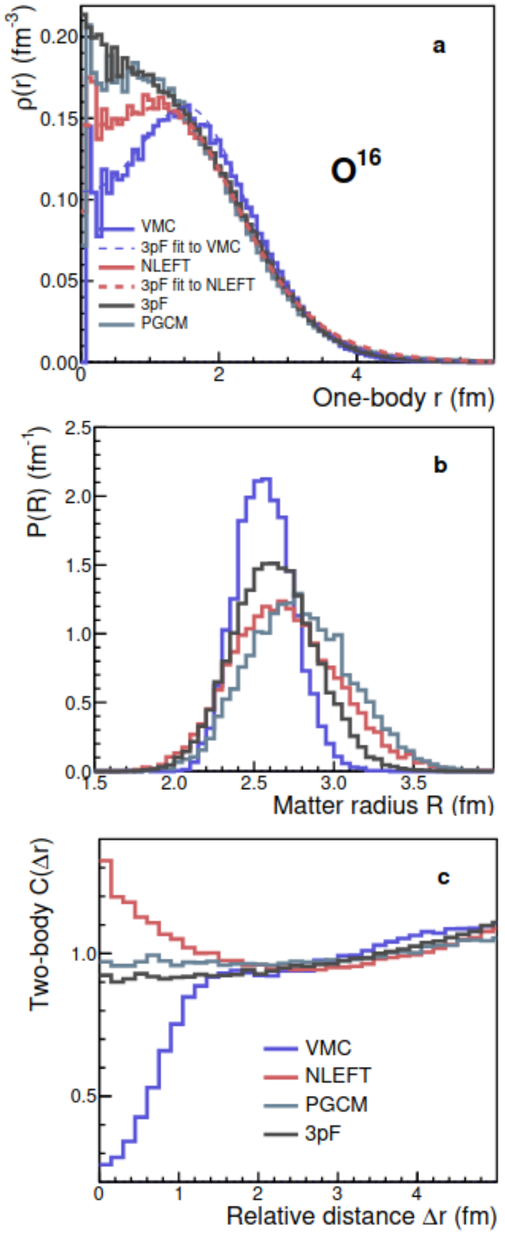

C.Zhang et al., PLB 862, 139322 (2025)

Clustering Model: Nucleon Configurations

❃ Acceptance-Rejection Method (ARM)

R.Christensen, A.Branscum, and T.E.Hanson, *Bayesian ideas and data analysis: an introduction for scientists and statisticians* (2010)

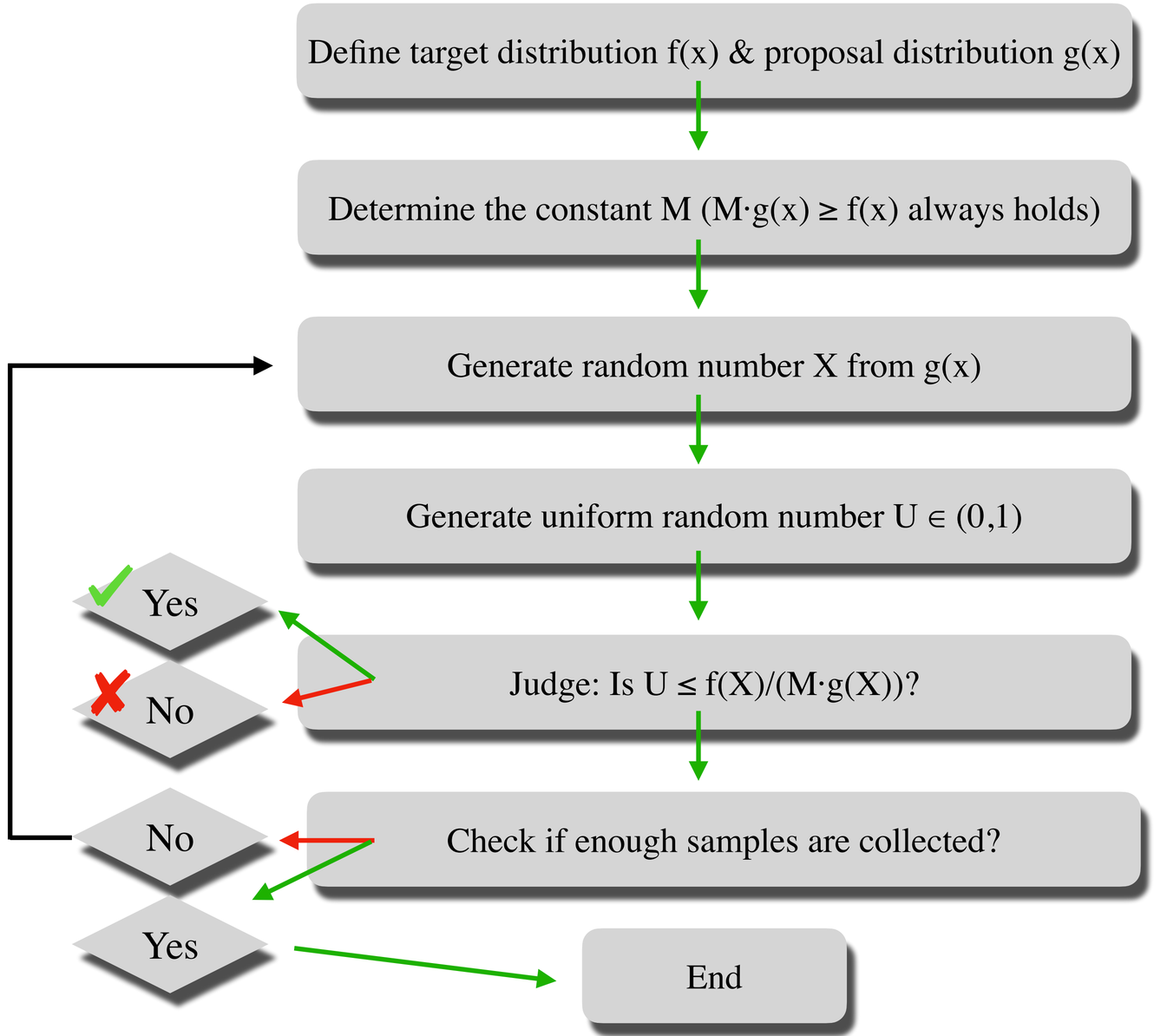

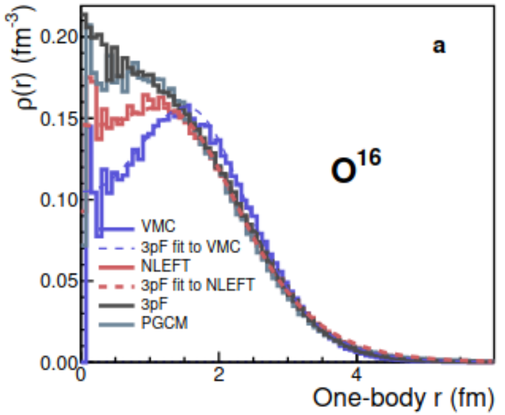

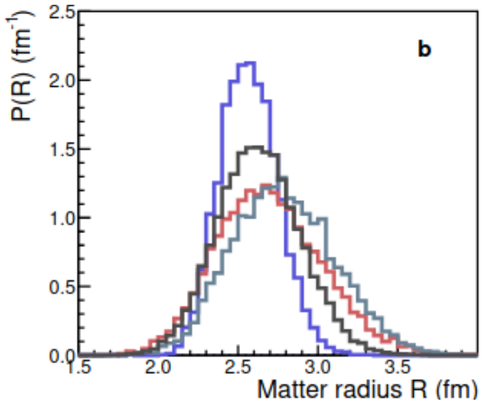

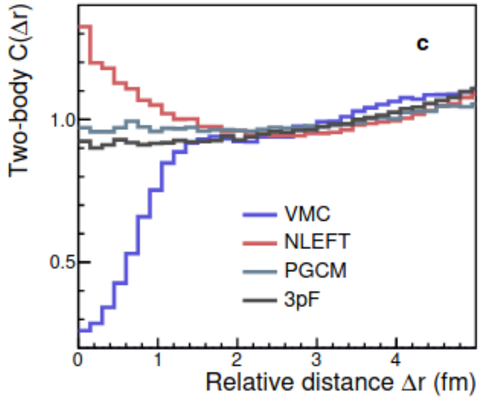

C.Zhang et al., PLB 862, 139322 (2025)

Clustering Model: Nucleon Configurations

❃ Acceptance-Rejection Method (ARM)

R.Christensen, A.Branscum, and T.E.Hanson, *Bayesian ideas and data analysis: an introduction for scientists and statisticians* (2010)

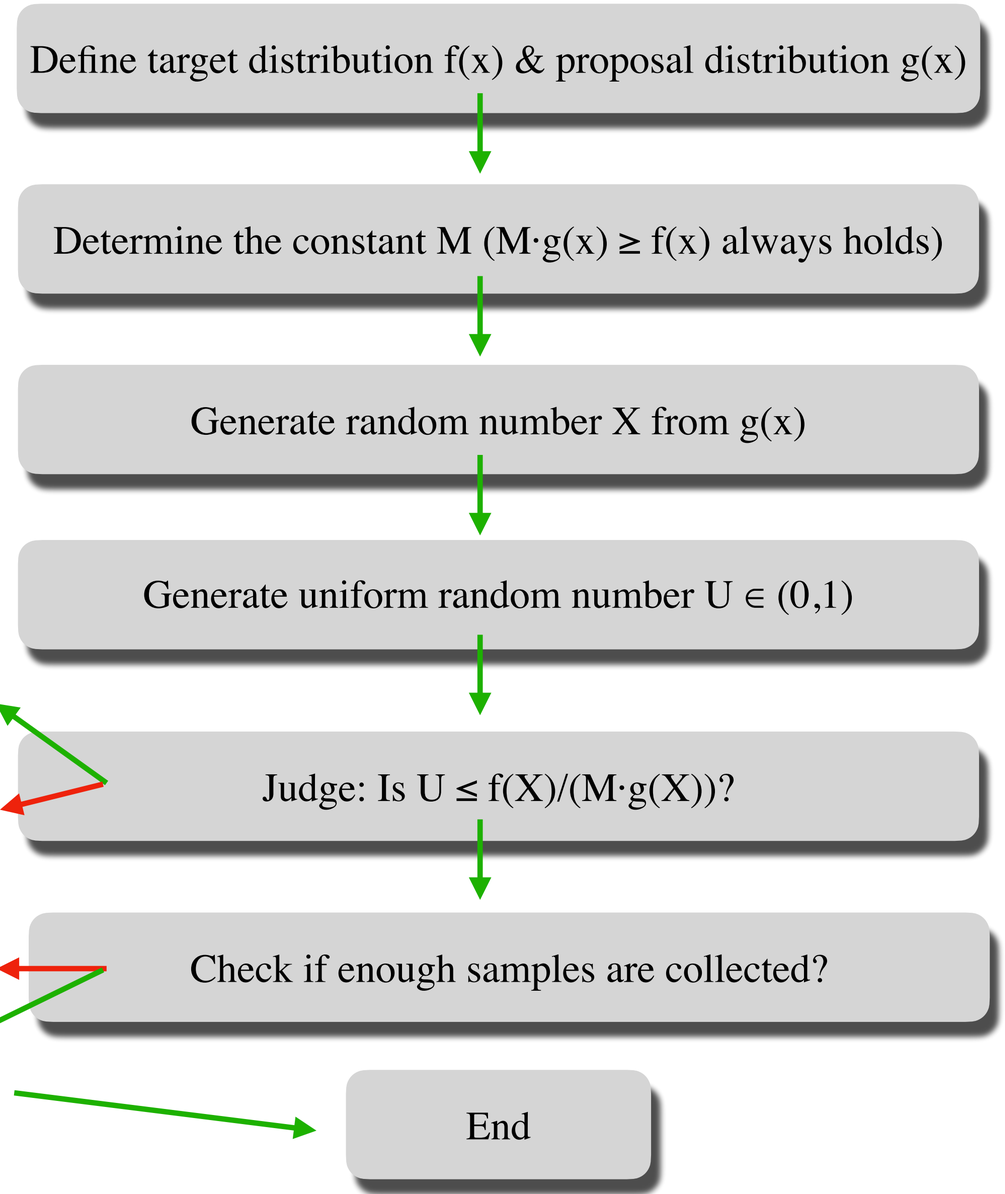

NN Correlations:

$$C(\Delta r) = 1 - \frac{\mathscr{F}(\Delta r)}{\mathscr{F}'(\Delta r)}$$

correlated

uncorrelated

❖ $f(x) = \mathscr{F}(\Delta r)$ & $g(x) = \mathscr{F}'(\Delta r)$

❖ Acceptance:

Q.Liu, HM, and B.Lu, 2509.00315

$$M = \sup_{\Delta r} \frac{\mathscr{F}(\Delta r)}{\mathscr{F}'(\Delta r)} = \Delta r_{biggest}$$

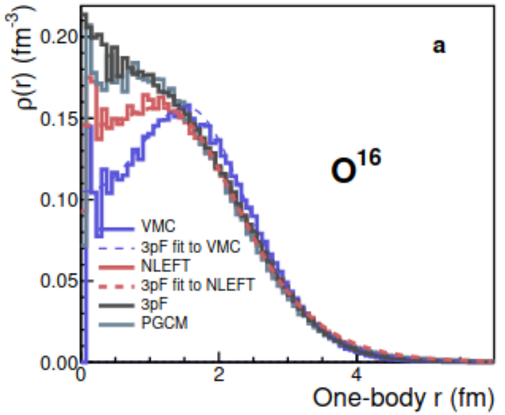

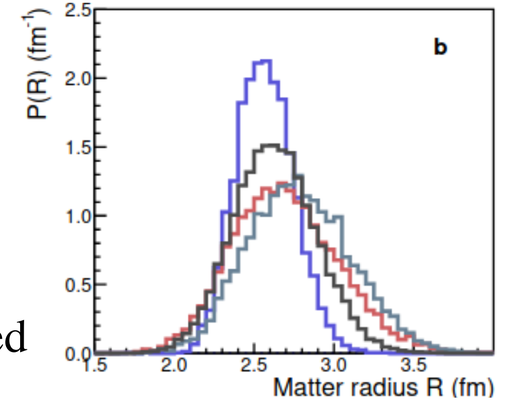

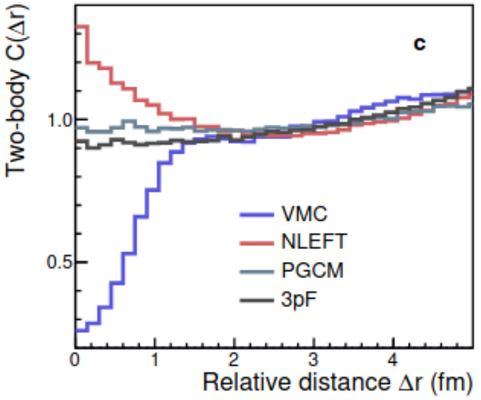

C.Zhang et al., PLB 862, 139322 (2025)

Isolated NN Correlations: O+O collisions

❃ Acceptance-Rejection Method (ARM) Q.Liu, HM, and B.Lu, 2509.00315

1. 3pF density distribution: $\rho(r) \propto \dfrac{1 + w\,(r^2/R_0^2)}{1 + e^{(r-R_0)/a_0}}$

2. Angle coordinates ($\cos\theta$ & ϕ) $\longrightarrow$ $\Delta r'$

3. $\mathscr{F}(\Delta r)$: NLEFT and VMC $\longrightarrow$ $M = \Delta r_{biggest}$

$$\longrightarrow U \leq \frac{\mathscr{F}(\Delta r')}{M \cdot \mathscr{F}'(\Delta r')}$$

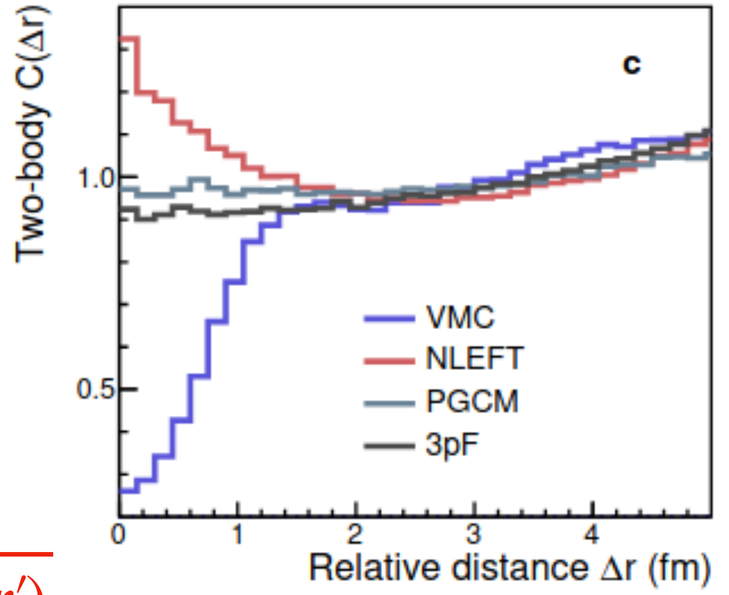

$R_0 = 2.608$ fm, $a_0 = 0.513$ fm, $w = -0.051$

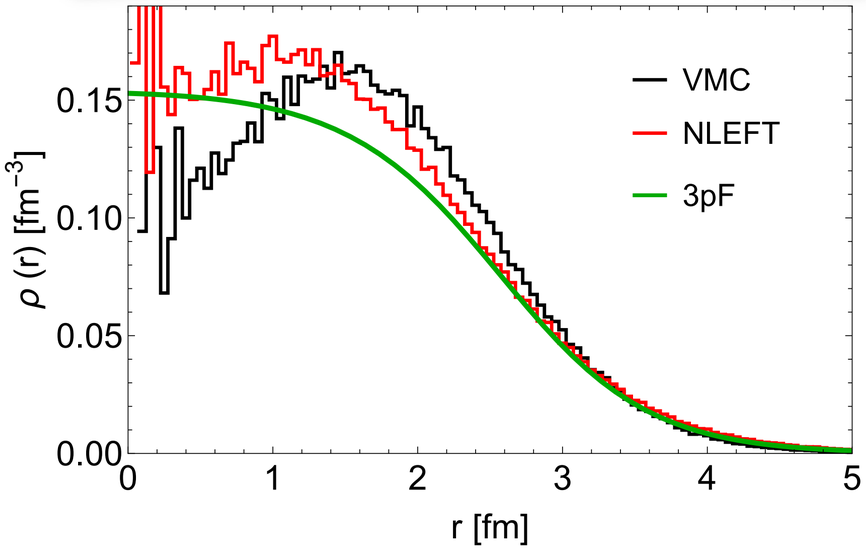

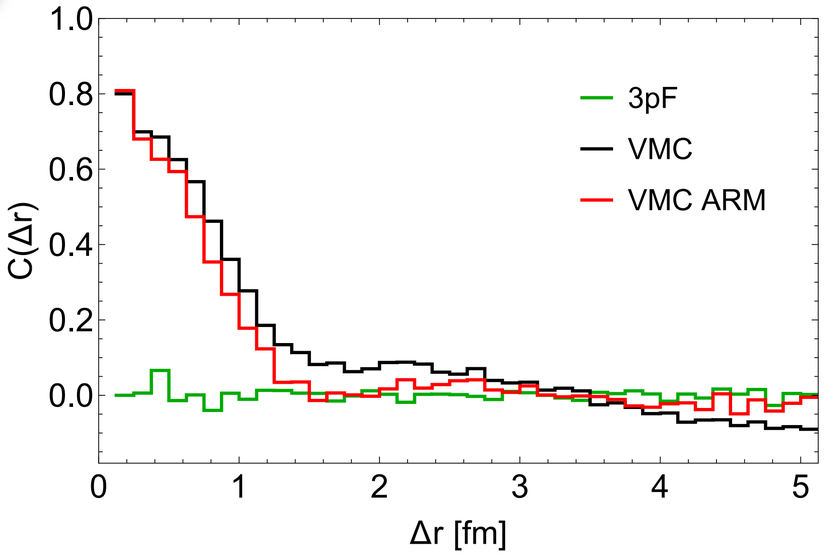

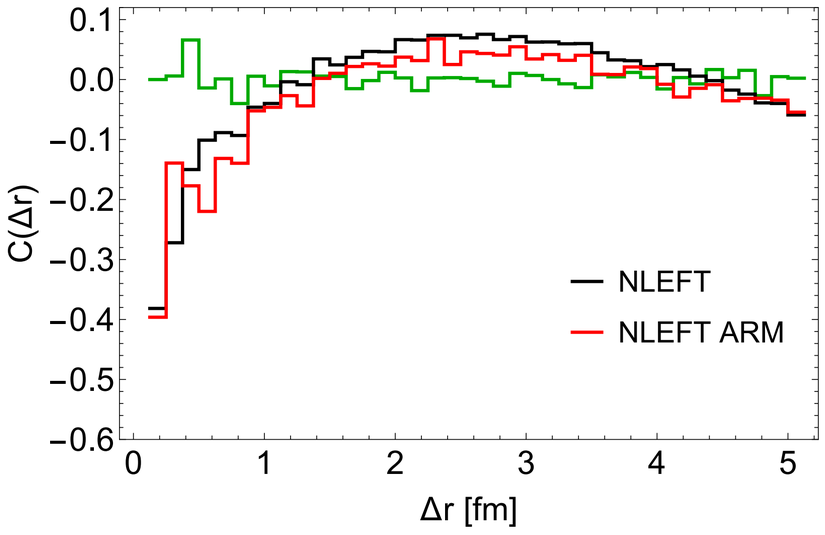

Isolated NN Correlations: O+O collisions

❃ Acceptance-Rejection Method (ARM) Q.Liu, HM, and B.Lu, 2509.00315

1. 3pF density distribution: $\rho(r) \propto \dfrac{1 + w\,(r^2/R_0^2)}{1 + e^{(r-R_0)/a_0}}$

2. Angle coordinates ($\cos\theta$ & ϕ) $\longrightarrow$ $\Delta r'$

3. $\mathscr{F}(\Delta r)$: NLEFT and VMC $\longrightarrow$ $M = \Delta r_{biggest}$

$\longrightarrow U \leq \dfrac{\mathscr{F}(\Delta r')}{M \cdot \mathscr{F}'(\Delta r')}$

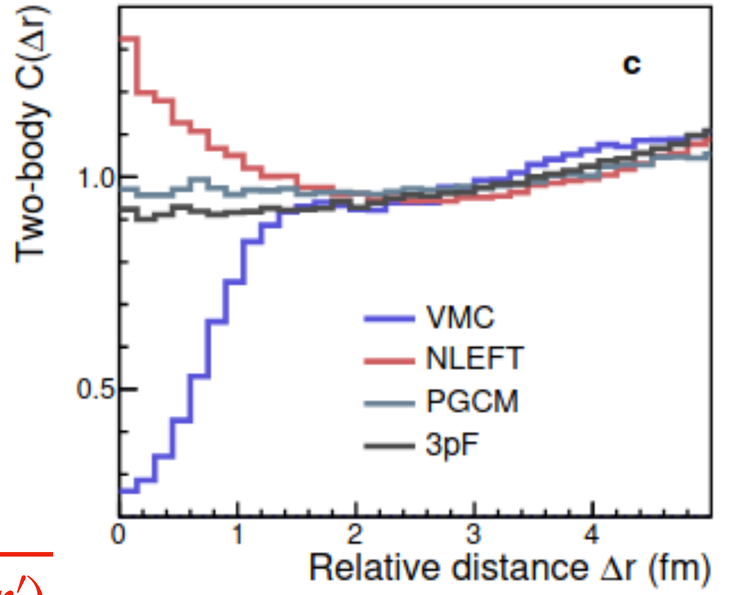

Angular Correlations

$R_0 = 2.608$ fm, $a_0 = 0.513$ fm, $w = -0.051$

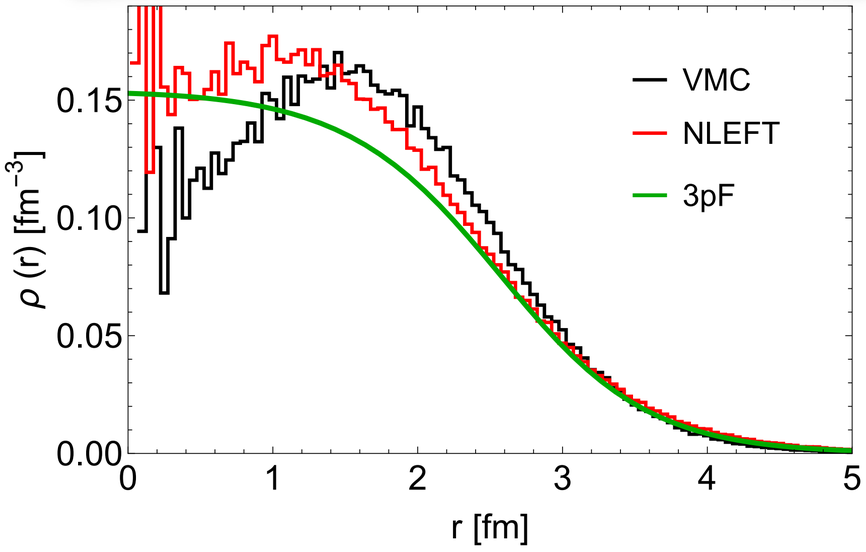

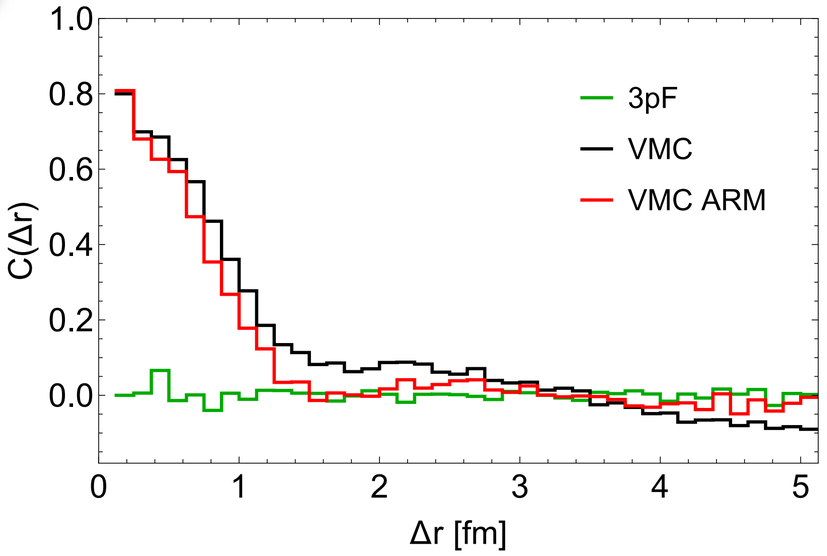

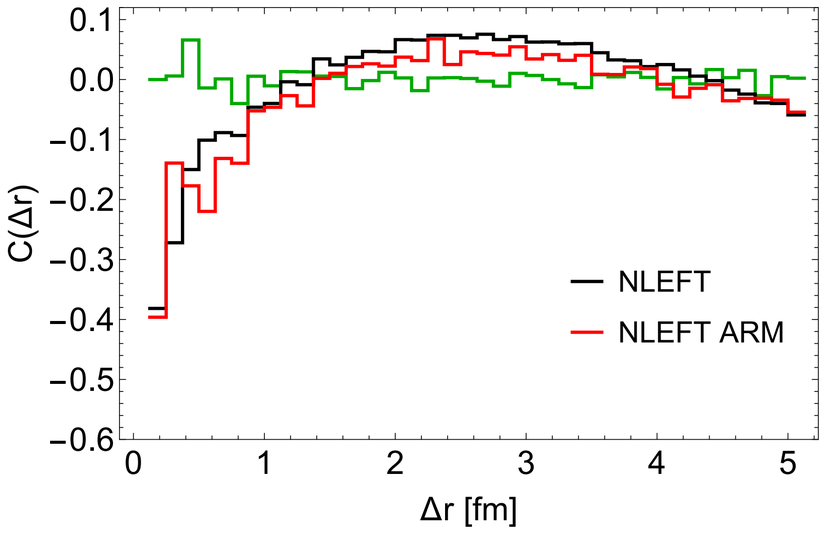

Angular Correlations: O+O collisions

Q.Liu, HM, and B.Lu, 2509.00315

$$\varepsilon_n\{2\}^2 = \frac{\int_{\mathbf{r}}\int_{\mathbf{r}'}|\mathbf{r}|^n|\mathbf{r}'|^n e^{ni(\phi-\phi')}\langle\delta\epsilon(\mathbf{r})\delta\epsilon(\mathbf{r}')\rangle_{ev}}{\left(\int_{\mathbf{r}}|\mathbf{r}|^n\langle\epsilon(\mathbf{r})\rangle_{ev}\right)^2} \rightarrow \delta\epsilon = \epsilon - \langle\epsilon\rangle$$

- The attractive correlation of NLEFT enhances fluctuations and $\varepsilon_n\{2\}$.
- The repulsion correlation of VMC reduces the eccentricities.

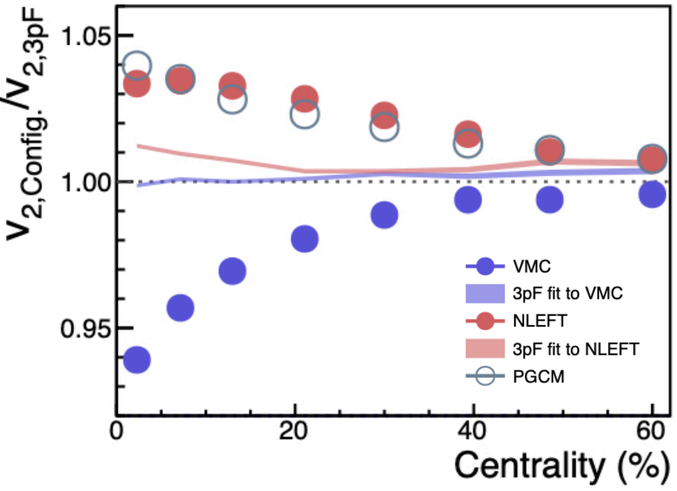

C.Zhang et al., PLB 862, 139322 (2025)

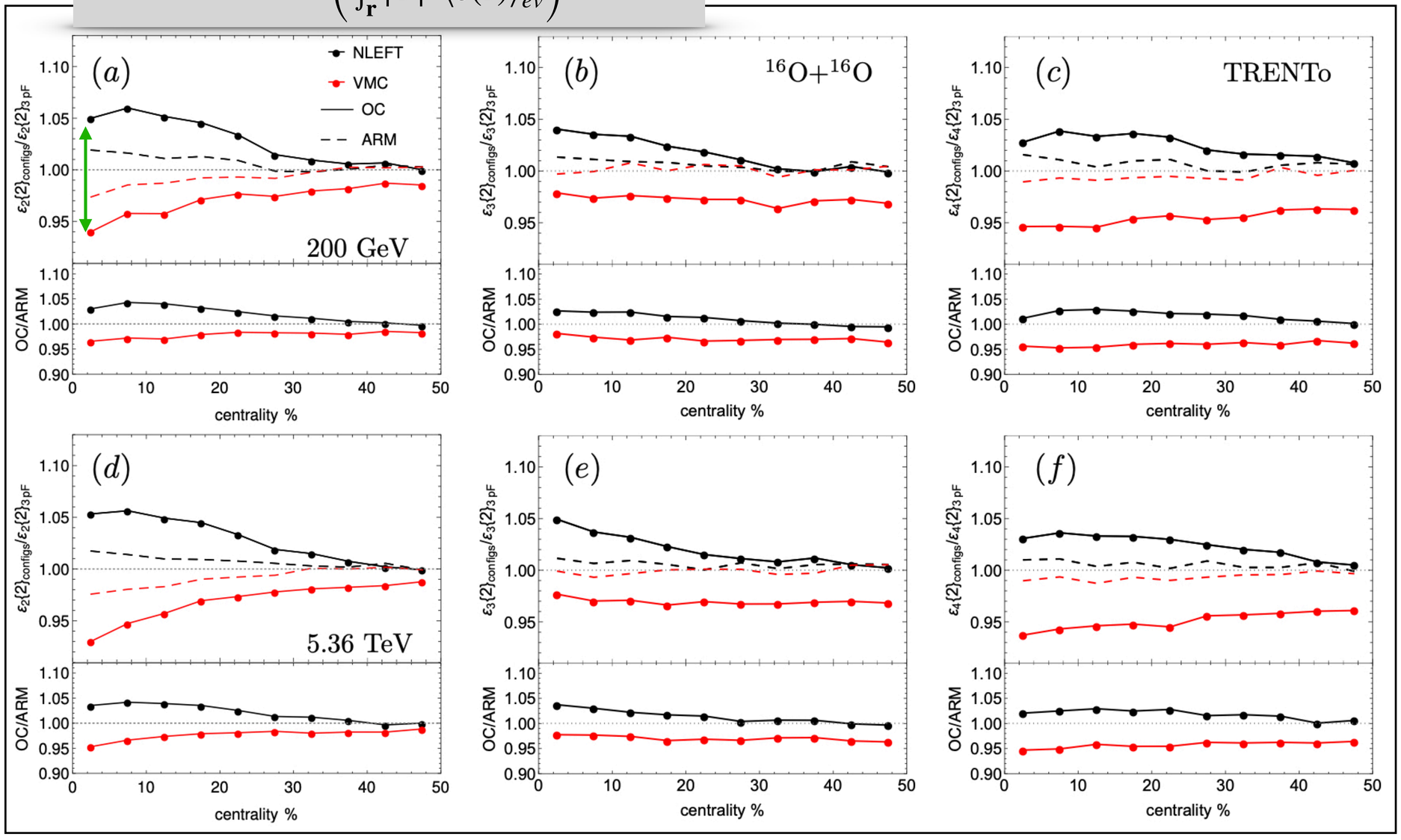

Angular Correlations: O+O collisions

Q.Liu, HM, and B.Lu, 2509.00315

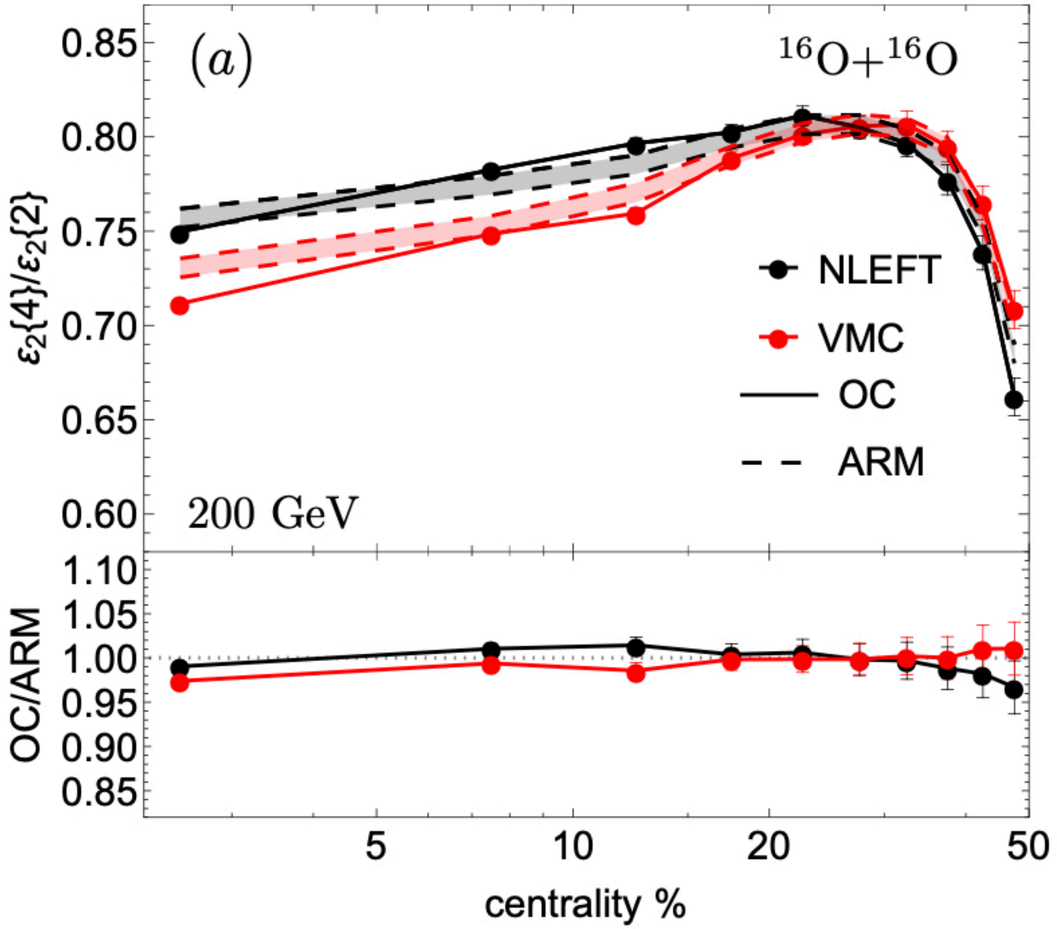

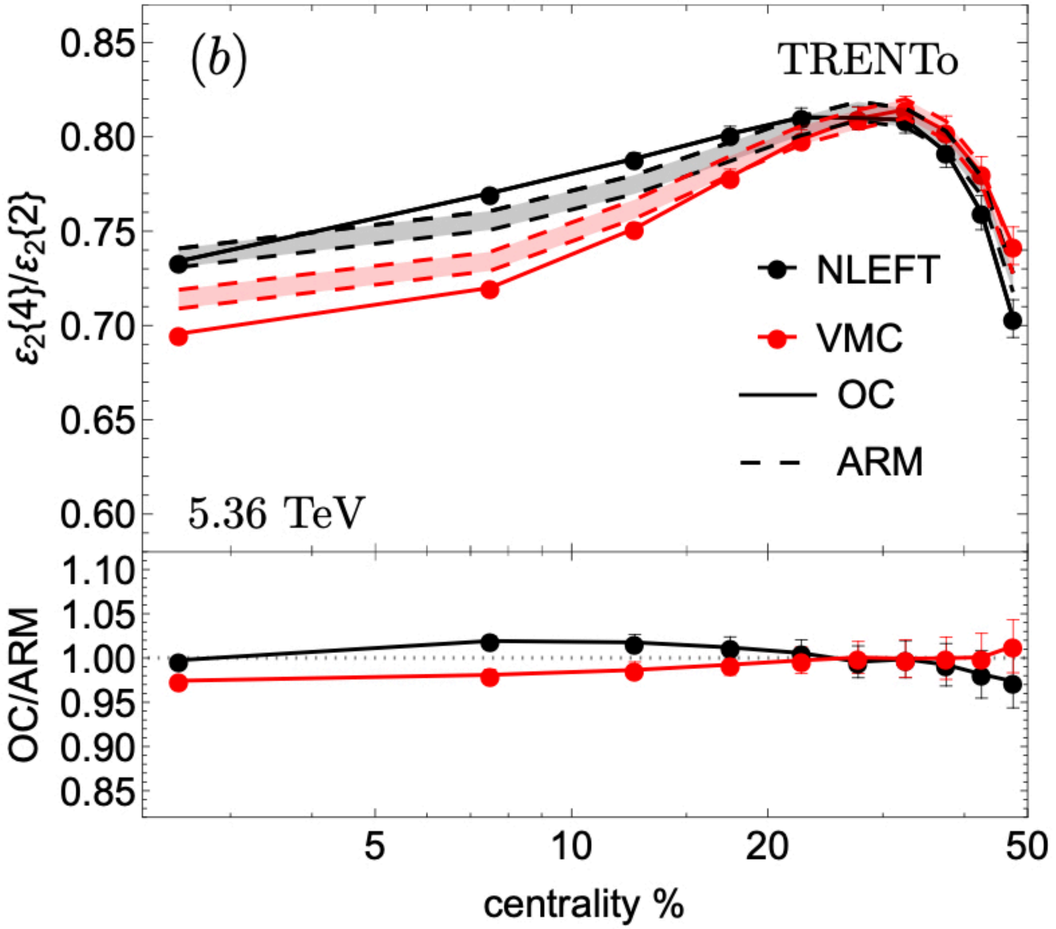

Alpha Clustering: O+O and Ne+Ne collisions

HM, PRC 113 (2026) 3, 034909

❃ Distribution of nucleons in each cluster

M.Rybczynski et al., PRC 97 (2018) 034912

$$\rho_\alpha(\vec{r}) = \left(\frac{3}{2\pi r_L^2}\right)^{3/2} \exp\left[-\frac{3(\vec{r}-\vec{L}_i)}{2r_L^2}\right]$$

$\vec{L}_i$: Position of the center of the cluster i

r_L: Root-mean-square radius of the clusters

1. Radial distribution (χ^2/NDF ≈ 1)

2. NN correlation distribution

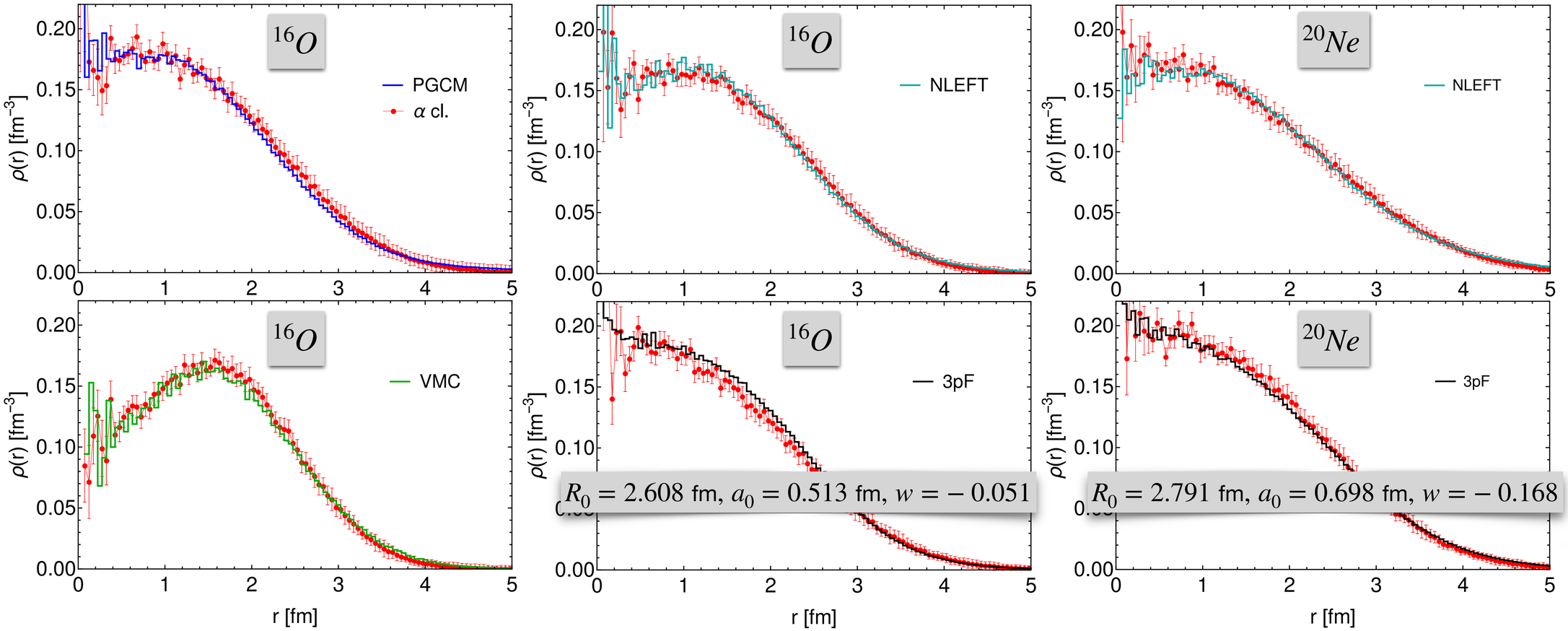

Tetrahedron

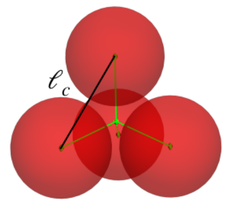

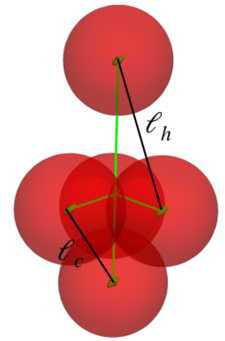

Bowlling-pin

Alpha Clustering: O+O and Ne+Ne collisions

HM, PRC 113 (2026) 3, 034909

❃ Distribution of nucleons in each cluster

M.Rybczynski et al., PRC 97 (2018) 034912

$$\rho_\alpha(\vec{r}) = \left(\frac{3}{2\pi r_L^2}\right)^{3/2} \exp\left[-\frac{3(\vec{r}-\vec{L}_i)}{2r_L^2}\right]$$

$\vec{L}_i$: Position of the center of the cluster i

r_L: Root-mean-square radius of the clusters

1. Radial distribution (χ^2/NDF ≈ 1)

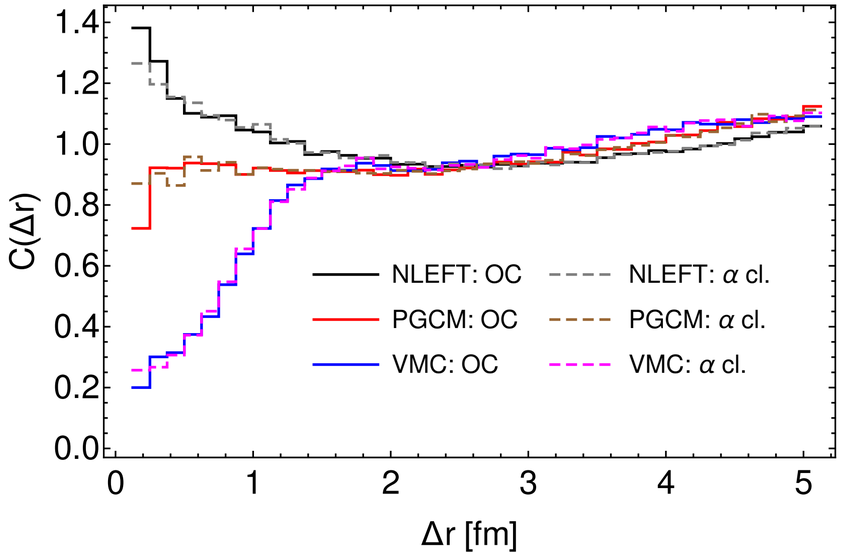

2. NN correlation distribution

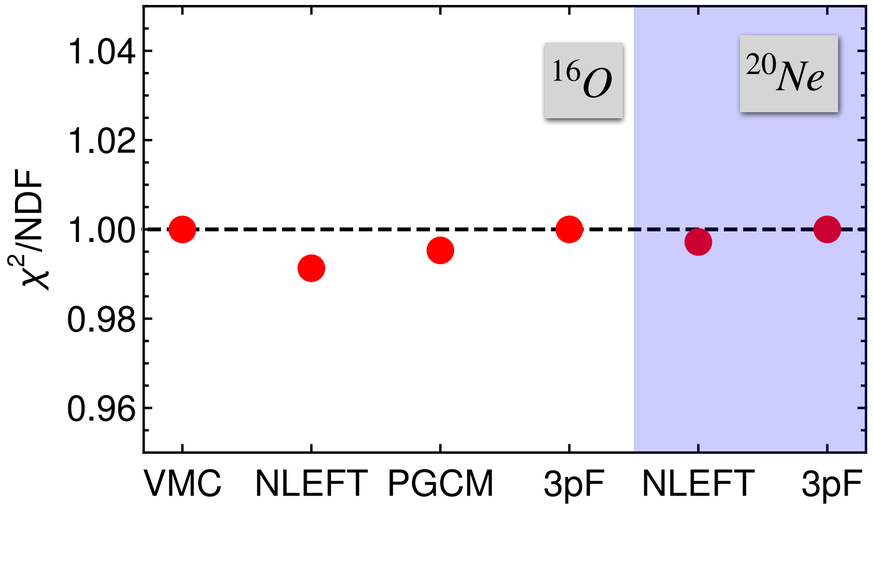

Tetrahedron

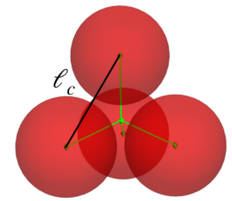

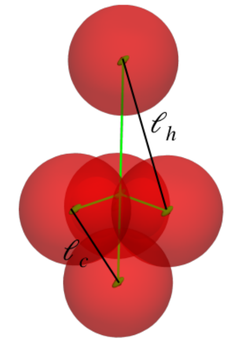

Bowlling-pin

Models	3pF	NLEFT	PGCM	VMC
(r_L, ℓ_c)				
^{16}O (RTP)	(1.83,3.20)	(1.84,3.17)	(1.88,3.06)	(1.52,3.26)
^{16}O (ITP)	(2.00,3.15)	(1.61,3.88)	(1.57,3.86)	-
(r_L, ℓ_c, ℓ_h)				
^{20}Ne (BP)	(2.00,3.00,3.00)	(2.20,3.00,3.50)	-	-

Alpha Clustering: O+O and Ne+Ne collisions

HM, PRC 113 (2026) 3, 034909

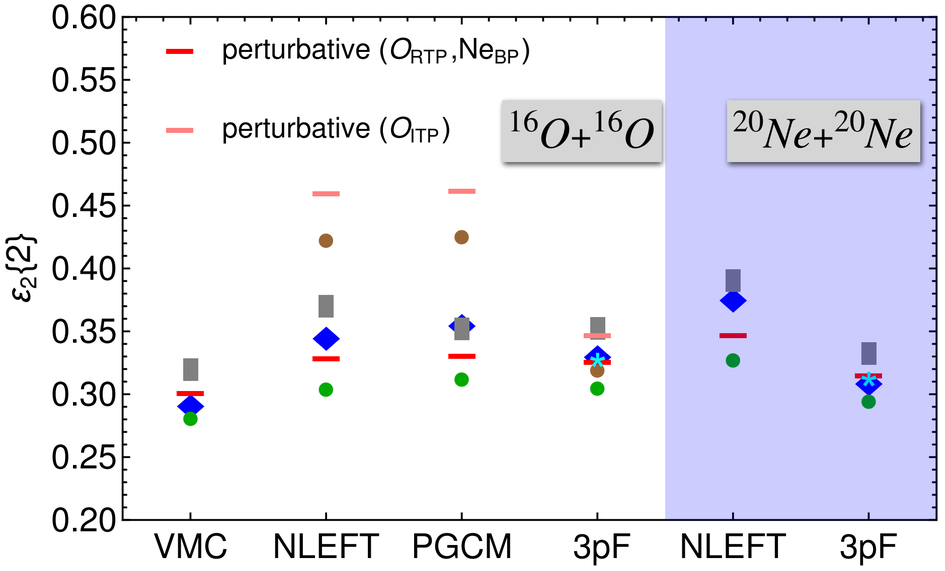

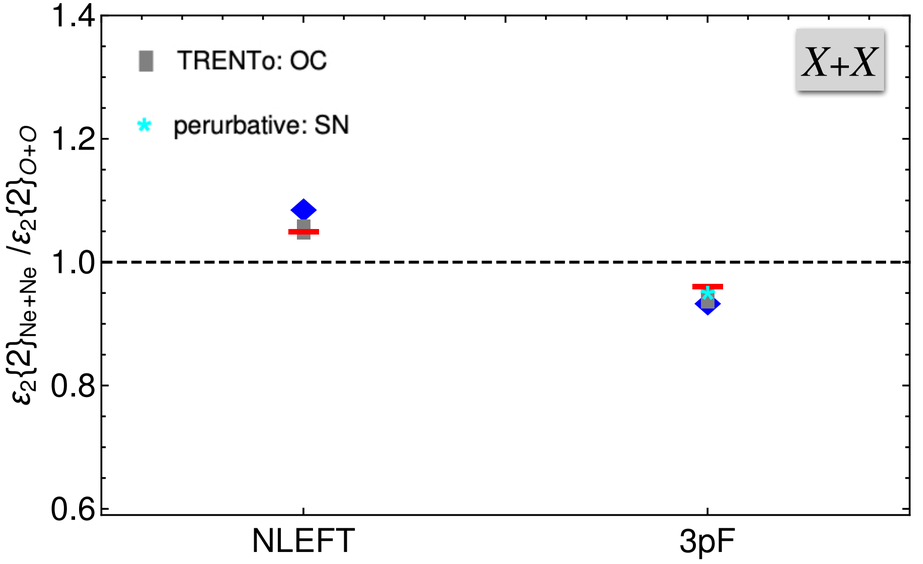

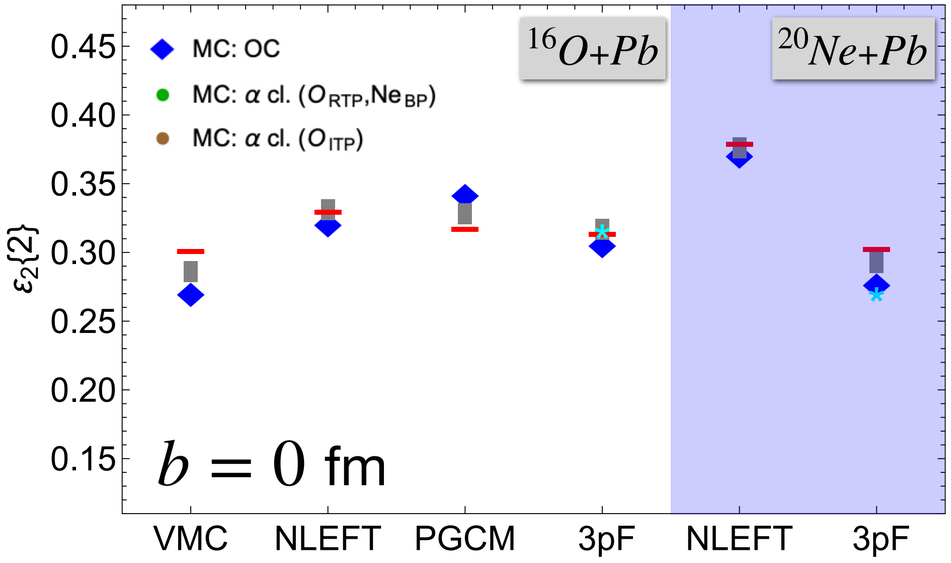

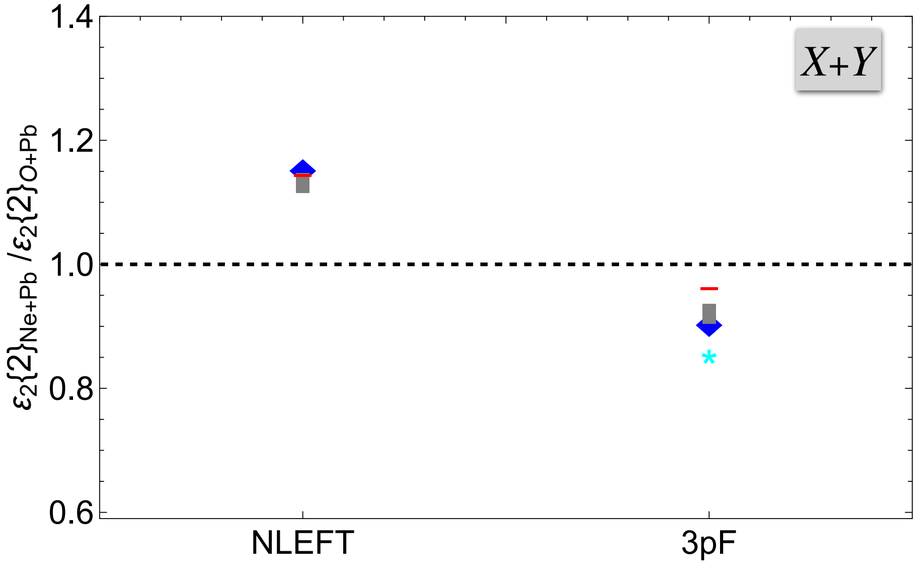

Spherical shape:

$$N(x,y,z) \propto e^{-\frac{3(x^2+y^2+z^2)}{2R_s^2}}$$

$$\xi = w^2/r_L^2 \;\&\; \eta = \ell_c^2/r_L^2$$

$$R_s = r_L\sqrt{\frac{1+3\xi}{\mathscr{P}(\eta,\xi)} - 3\xi}$$

Alpha Clustering: O+O and Ne+Ne collisions

HM, PRC 113 (2026) 3, 034909

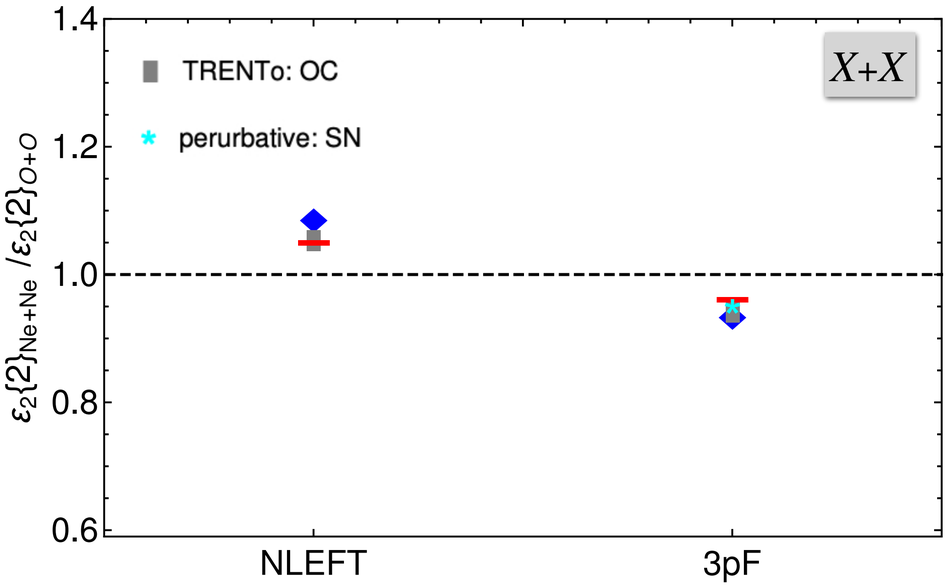

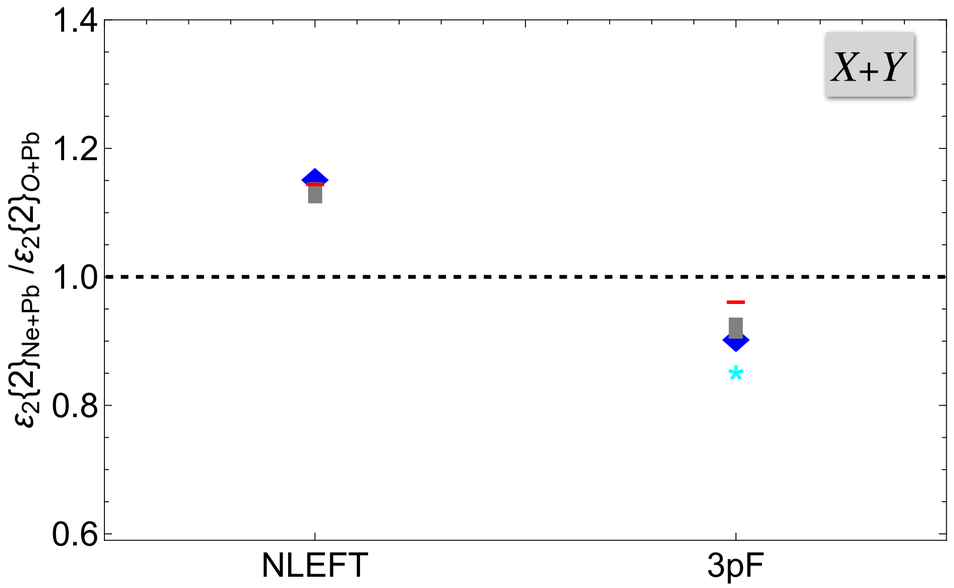

$$\frac{Pb+Ne}{Pb+O} \approx 1.19$$

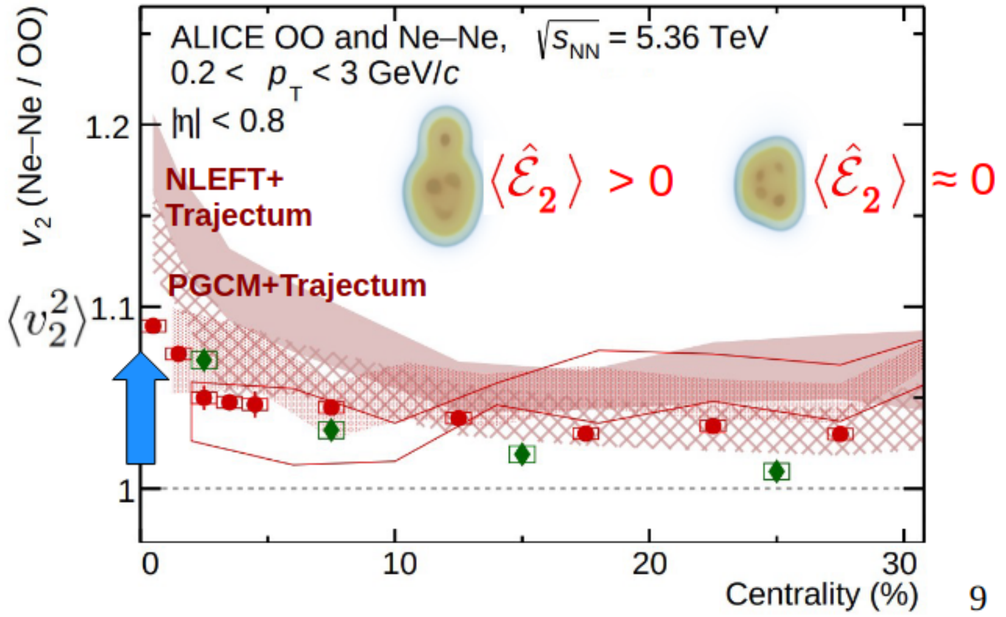

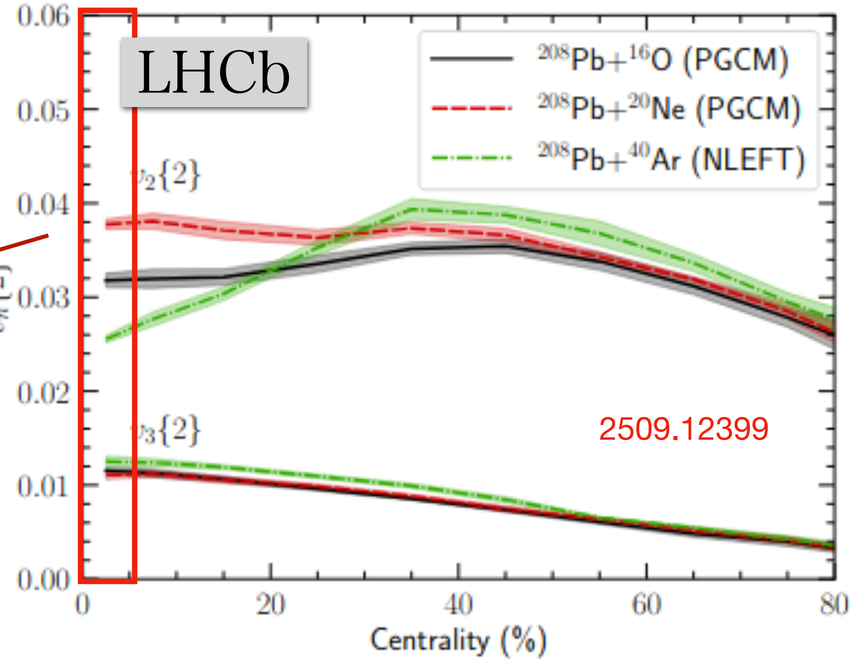

Alpha Clustering: Different Shapes

HM, PRC 113 (2026) 3, 034909

(r_L, ℓ_c, ℓ_h)

Models	3pF	NLEFT	PGCM	VMC
^{16}O (RTP)	(1.83,3.20)	(1.84,3.17)	(1.88,3.06)	(1.52,3.26)
^{16}O (ITP)	(2.00,3.15)	(1.61,3.88)	(1.57,3.86)	-
^{20}Ne (BP)	(2.00,3.00,3.00)	(2.20,3.00,3.50)	-	-

$\ell_h \approx 0.52\, \ell_c$ NLEFT & PGCM

$\ell_h \approx 0.9\, \ell_c$ 3pF

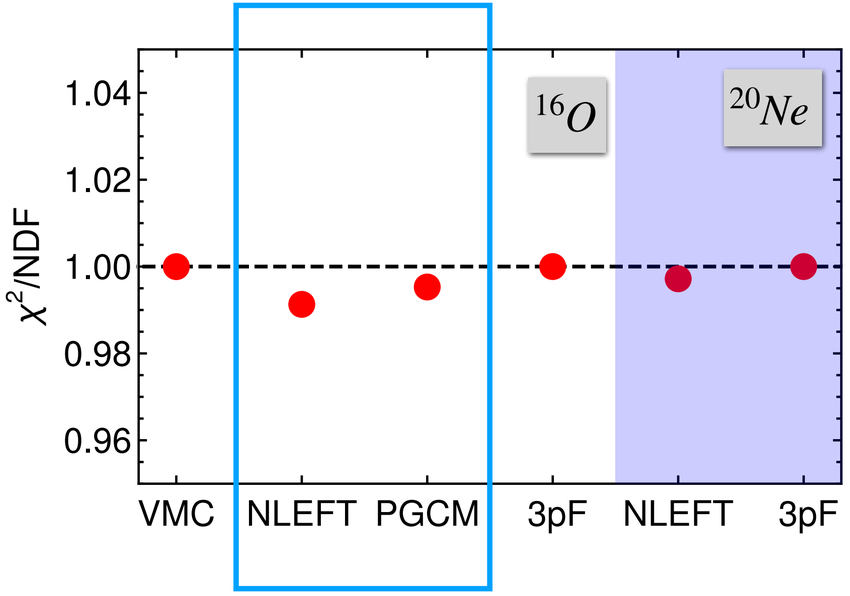

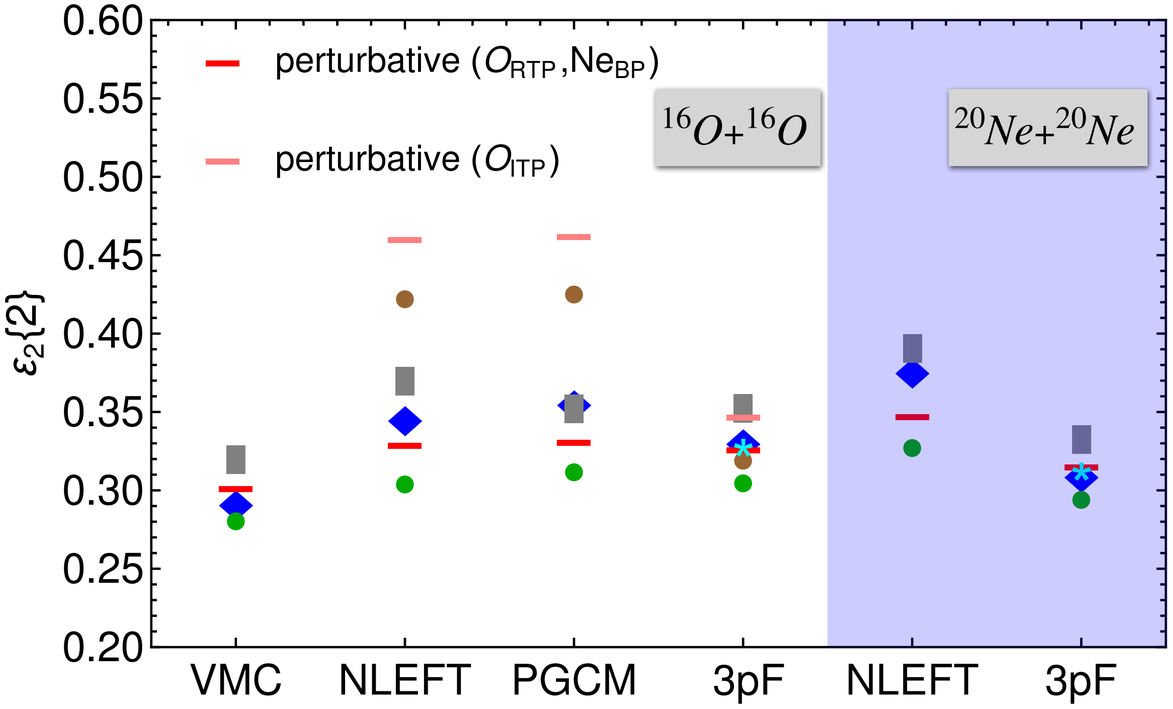

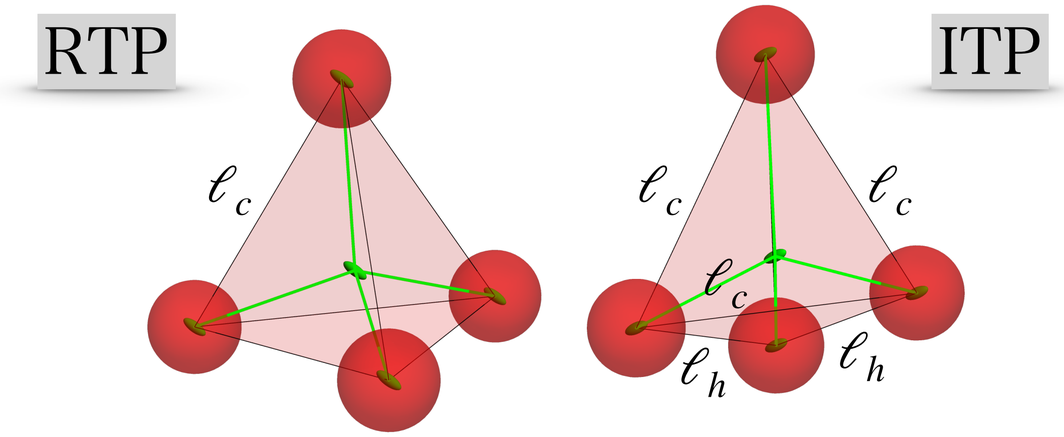

Alpha Clustering: Different Shapes

HM, PRC 113 (2026) 3, 034909

(r_L, ℓ_c, ℓ_h)

Models	3pF	NLEFT	PGCM	VMC
^{16}O (RTP)	(1.83,3.20)	(1.84,3.17)	(1.88,3.06)	(1.52,3.26)
^{16}O (ITP)	(2.00,3.15)	(1.61,3.88)	(1.57,3.86)	-
^{20}Ne (BP)	(2.00,3.00,3.00)	(2.20,3.00,3.50)	-	-

$\ell_h \approx 0.52\, \ell_c$ NLEFT & PGCM

$\ell_h \approx 0.9\, \ell_c$ 3pF

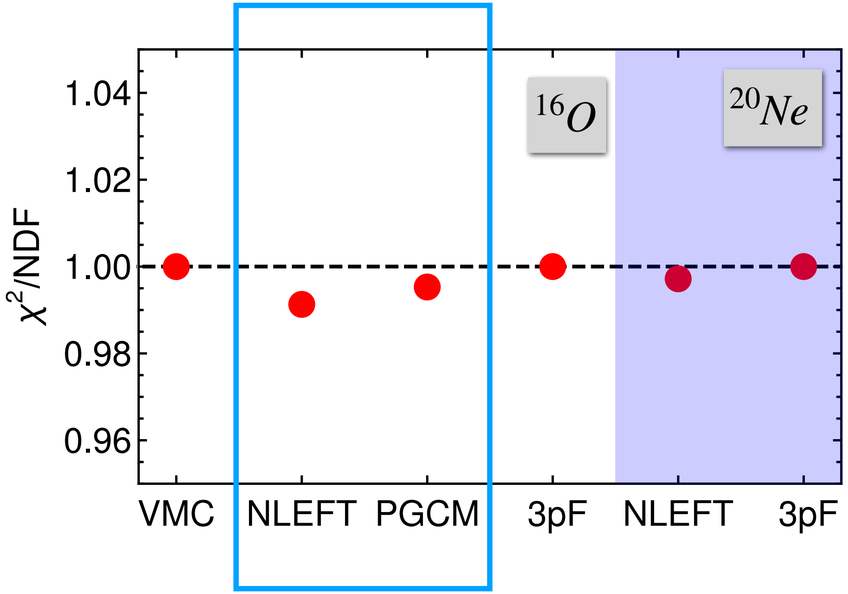

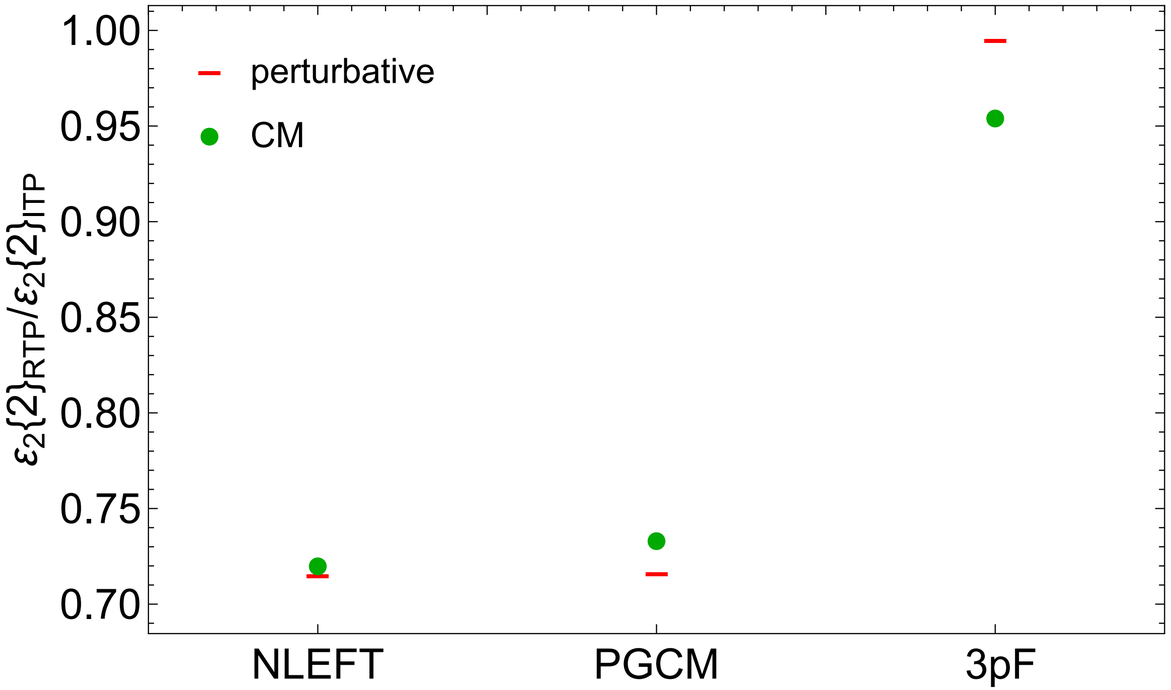

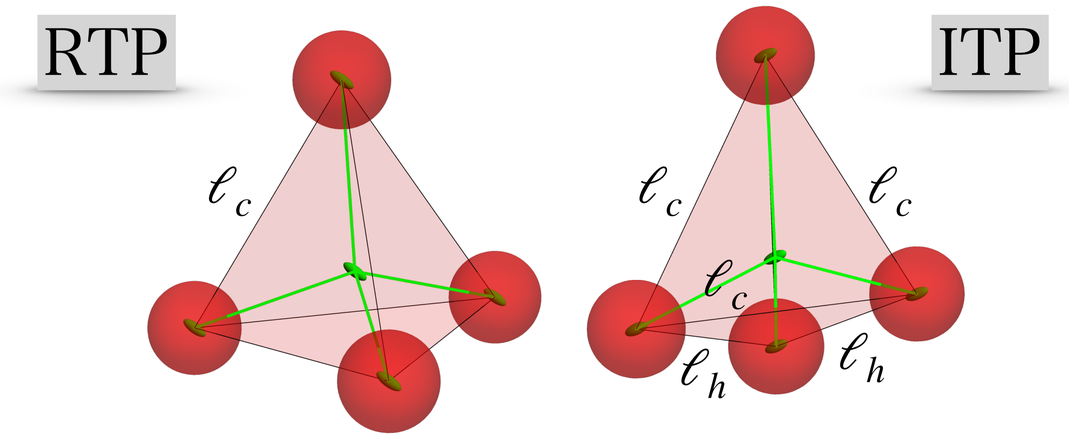

Summery

- A general theoretical picture: from light to heavy nuclei
- Symmetric and asymmetric collisions
- Acceptance-rejection method
- Imprints of isolated nucleon-nucleon correlations
- Angular correlations
- Imprint of ***ab initio*** correlations within a clustering model
- Reproduced differences between the structures of Neon-20 and Oxygen-16

Summery

- A general theoretical picture: from light to heavy nuclei
- Symmetric and asymmetric collisions
- Acceptance-rejection method
- Imprints of isolated nucleon-nucleon correlations
- Angular correlations
- Imprint of ***ab initio*** correlations within a clustering model
- Reproduced differences between the structures of Neon-20 and Oxygen-16

Thanks For Your Attention!

BACKUP

Many-Body Operators

HM, G.Giacalone, M.Luzum, 2604.00619

Nuclear density:

$$G(r,\theta,\phi) = \frac{1}{(2\pi)^{3/2}R_0^3}\exp(-r^2/2R(\theta,\phi)^2),$$

with

$$R(\theta,\phi) = R_0(1+\beta_2[\cos\gamma Y_2^0(\theta,\phi) + \sin\gamma Y_2^2(\theta,\phi)])\boxed{-\frac{\beta_2^2}{4\pi}}$$

$$\int N(r,\theta,\phi)\, r^2\sin(\theta)\, dr\, d\theta\, d\phi = 1$$

$$\mathscr{Y}(\theta,\phi) = \cos\gamma Y_2^0(\theta,\phi) + \sin\gamma Y_2^2(\theta,\phi)$$

Expansion:

$$N(r,\theta,\phi) = \frac{e^{-\frac{r^2}{2R_0^2}}}{2\sqrt{2}\pi^{3/2}R_0^3}\left[1+\beta_2\frac{\mathscr{Y}(\theta,\phi)r^2}{R_0^2} + \beta_2^2\frac{2\pi\mathscr{Y}(\theta,\phi)^2r^4 - r^2R_0^2(1+6\pi\mathscr{Y}(\theta,\phi)^2)}{4\pi R_0^4} + \cdots\right]$$

$$\langle r_\perp^2\rangle = \int_{\mathbf{r}_\perp}\rho_\perp^{(1)}(\mathbf{r}_\perp)\, r_\perp^2 = 2R_0^2\left(1+\frac{5}{4\pi}\beta_2^2\right)$$

$$\left\langle r_{1\perp}^n r_{2\perp}^n e^{in(\phi_1-\phi_2)}\right\rangle = \int_{\mathbf{r}_{1\perp},\mathbf{r}_{2\perp}}\rho_\perp^{(2)}(\mathbf{r}_{1\perp},\mathbf{r}_{2\perp})\, r_{1\perp}^n r_{2\perp}^n e^{in(\phi_1-\phi_2)} = \frac{6R_0^4}{\pi}\beta_2^2 + \frac{24\sqrt{5}R_0^4}{7\pi^{3/2}}\beta_2^3\cos(3\gamma)$$

$$\left\langle r_{1\perp}^2 r_{2\perp}^2 r_{3\perp}^2 e^{i2(\phi_2-\phi_3)}\right\rangle = \int_{\mathbf{r}_{1\perp},\mathbf{r}_{2\perp},\mathbf{r}_{3\perp}}\rho_\perp^{(3)}(\mathbf{r}_{1\perp},\mathbf{r}_{2\perp},\mathbf{r}_{3\perp})\, r_{1\perp}^2 r_{2\perp}^2 r_{3\perp}^2 e^{i2(\phi_2-\phi_3)} = \frac{12R_0^6}{\pi}\beta_2^2 + \frac{60\sqrt{5}R_0^6}{7\pi^{3/2}}\beta_2^3\cos(3\gamma)$$

$$\left\langle r_{1\perp}^2 r_{2\perp}^2 r_{3\perp}^2 e^{i2(\phi_2-\phi_3)}\right\rangle - \left\langle r_\perp^2\right\rangle\left\langle r_{1\perp}^2 r_{2\perp}^2 e^{i2(\phi_1-\phi_2)}\right\rangle = \frac{12\sqrt{5}R_0^6}{7\pi^{3/2}}\beta_2^3\cos(3\gamma)$$

Two-Body Correlators

HM, PRC 113 (2026) 3, 034909

Variance of energy density: $\mathrm{var}(E/\langle E\rangle) = \dfrac{\langle E^2\rangle_{ev}}{\langle E\rangle_{ev}^2} - 1 = \dfrac{\int_\Omega \int_{\Omega'} \langle E(\Omega,\Omega')^2\rangle}{\int_\Omega \int_{\Omega'} \langle E(\Omega,\Omega')\rangle^2} - 1$

Two point function:

$$
\begin{aligned}
&\langle \epsilon(\mathbf{r},\Omega,\Omega')\epsilon(\mathbf{r}',\Omega,\Omega')\rangle \\
&= AB \sum_{i,i'}^{N_\alpha} H_i^{(P)}(\mathbf{r},\mathbf{r}',\Omega) H_{i'}^{(T)}(\mathbf{r},\mathbf{r}',\Omega') \\
&+ 2A(B^2-B) \sum_{i,i'}^{N_\alpha} H_i^{(P)}(\mathbf{r},\mathbf{r}',\Omega) H_{i'i'}^{(T)}(\mathbf{r},\mathbf{r}',\Omega') \\
&+ 2AB^2 \sum_{i,i'\neq j'}^{N_\alpha} H_i^{(P)}(\mathbf{r},\mathbf{r}',\Omega) H_{i'j'}^{(T)}(\mathbf{r},\mathbf{r}',\Omega') \\
&+ 2A^2(B^2-B) \sum_{i\neq j,i'}^{N_\alpha} H_{ij}^{(P)}(\mathbf{r},\mathbf{r}',\Omega) H_{i'i'}^{(T)}(\mathbf{r},\mathbf{r}',\Omega') \\
&+ A^2B^2 \sum_{i\neq j,i'\neq j'}^{N_\alpha} H_{ij}^{(P)}(\mathbf{r},\mathbf{r}',\Omega) H_{i'j'}^{(T)}(\mathbf{r},\mathbf{r}',\Omega') \\
&+ (A^2-A)(B^2-B) \sum_{i,i'}^{N_\alpha} H_{ii}^{(P)}(\mathbf{r},\mathbf{r}',\Omega) H_{i'i'}^{(T)}(\mathbf{r},\mathbf{r}',\Omega').
\end{aligned}
$$

$$
\begin{aligned}
\langle E\rangle_{ev} &= \int_\Omega \int_{\Omega'} \langle E(\Omega,\Omega')\rangle \\
&= \frac{3A^2 \sum_{i,j=1}^{N_\alpha} 1_{ij}}{4\pi r_L^2(1+3\xi)} \left[1 + \sum_{n=1} \frac{(-\eta)^n b_n}{(1+3\xi)^n}\right] \\
&= \frac{3A^2N_\alpha^2}{4\pi r_L^2(1+3\xi)} \left[1 + \sum_{n=1} \frac{(-\eta)^n b_n}{(1+3\xi)^n}\right],
\end{aligned}
$$

$b_1 = 1/8,$
$b_2 = 1/20,$
$\vdots$

$\xi = w^2/r_L^2$ & $\eta = \ell_c^2/r_L^2$

$$
\begin{aligned}
\langle E^2\rangle_{ev} &= \int_\Omega \int_{\Omega'} \langle E(\Omega,\Omega')^2\rangle \\
&= \frac{3A^2N_\alpha^2}{16\pi^2 r_L^4 (2+3\xi)\,\xi} \mathcal{P}_1(\eta,\xi) \\
&+ \frac{3(A-1)A^2N_\alpha^2}{4\pi^2 r_L^4 (1+8\xi+12\xi^2)} \mathcal{P}_2(\eta,\xi) \\
&+ \frac{3A^3N_\alpha^2(N_\alpha-1)}{4\pi^2 r_L^4 (1+8\xi+12\xi^2)} \mathcal{P}_3(\eta,\xi) \\
&+ \frac{9(A-1)^2A^2N_\alpha^2(N_\alpha-1)}{16\pi^2 r_L^4 (1+3\xi)^2} \mathcal{P}_4(\eta,\xi) \\
&+ \frac{9A^3N_\alpha^2(N_\alpha-1)^2}{16\pi^2 r_L^4 (1+3\xi)^2} \mathcal{P}_5(\eta,\xi) \\
&+ \frac{9(A-1)A^3N_\alpha^2}{8\pi^2 r_L^4 (1+3\xi)^2} \mathcal{P}_6(\eta,\xi),
\end{aligned}
$$

$$
\begin{aligned}
\mathcal{P}_1(\eta,\xi) &= \left[1 + \sum_{n=1} \frac{(-\eta)^n d_n^{(1)}}{(2+3\xi)^n}\right], \\
\mathcal{P}_2(\eta,\xi) &= \left[1 + \sum_{n=1} \frac{(-\eta)^n d_n^{(2)}}{(1+2\xi)^n}\right], \\
&\vdots
\end{aligned}
$$